



HAL
open science

Self-Assembly of Stimuli-Responsive Biohybrid Synthetic-b-Recombinant Block Copolypeptides

Gaëlle Le Fer, Anne-Laure Wirotius, Annie Brûlet, Elisabeth Garanger,
Sébastien Lecommandoux

► **To cite this version:**

Gaëlle Le Fer, Anne-Laure Wirotius, Annie Brûlet, Elisabeth Garanger, Sébastien Lecommandoux. Self-Assembly of Stimuli-Responsive Biohybrid Synthetic-b-Recombinant Block Copolypeptides. *Biomacromolecules*, 2019, 20 (1), pp.254-272. 10.1021/acs.biomac.8b01390 . hal-01948441

HAL Id: hal-01948441

<https://hal.science/hal-01948441>

Submitted on 8 Jul 2019

HAL is a multi-disciplinary open access archive for the deposit and dissemination of scientific research documents, whether they are published or not. The documents may come from teaching and research institutions in France or abroad, or from public or private research centers.

L'archive ouverte pluridisciplinaire **HAL**, est destinée au dépôt et à la diffusion de documents scientifiques de niveau recherche, publiés ou non, émanant des établissements d'enseignement et de recherche français ou étrangers, des laboratoires publics ou privés.

Self-assembly of stimuli-responsive biohybrid synthetic-*b*-recombinant block copolypeptides

Gaëlle Le Fer^{§†}, Anne-Laure Wirocius^{§†}, Annie Brûlet[‡], Elisabeth Garanger^{§†}, Sébastien Lecommandoux^{*§†}

§ Université de Bordeaux, Bordeaux INP, ENSCBP, 16 avenue Pey-Berland, 33607 Pessac

Cedex, France, † CNRS, Laboratoire de Chimie des Polymères Organiques (UMR5629), Pessac,

France, ‡ Laboratoire Léon Brillouin, UMR 12 CEA–CNRS, CEA Saclay, 91191 Gif-sur-Yvette

Cedex, France.

KEYWORDS: elastin-like polypeptides, poly(*L*-glutamic acid), thermoresponsive diblock copolypeptides, self-assembly, nanoparticles.

ABSTRACT. The synthesis and original thermoresponsive behavior of hybrid diblock copolypeptides composed of synthetic and recombinant polypeptides are herein reported. A thermoresponsive recombinant elastin-like polypeptide was used as macroinitiator to synthesize a range of poly(*L*-glutamic acid)-*block*-elastin-like polypeptide (PGlu-*b*-ELP) diblock copolypeptides with variable PGlu block lengths. Their temperature-triggered self-assembly in water and in phosphate-buffered saline (PBS) was investigated at the macroscopic scale using complementary techniques such as turbidimetry, dynamic and static light scattering, small-angle

neutron scattering, and at the molecular scale by ^1H NMR and circular dichroism (CD). In deionized water, PGlu-*b*-ELP copolypeptides showed one transition from free soluble chains below the transition temperature (T_t) of the ELP block to macroscopic aggregates above the T_t . In contrast, in PBS, four successive regimes were observed upon increasing temperature: below the T_t , copolypeptides were soluble, above the T_t , large aggregates appeared and fell apart into discrete and defined spherical nanoparticles at a temperature named critical micellization temperature (CMT), before finally reaching an equilibrium. During the last regime, neutron scattering experiments revealed that the micelle-like structures underwent a densification step and expelled water from their core. In addition, ^1H NMR and CD experiments revealed, in deionized water, the formation of type II β -turns into the ELP block upon temperature increase. These β -turns are known to participate in the intrinsic thermoresponsive behavior of the ELPs. In contrast, in PBS, circular dichroism measurements showed an attenuation of folded structure during the self-assembly phase, leading to less cohesive aggregates able to reorganize into nanoparticles at the CMT.

Introduction

Interest in thermoresponsive polymers has steadily grown over the past decades, and numerous studies have been dedicated to the design of smart temperature-sensitive macromolecules for a large variety of applications.¹⁻⁴ Within this family, are the polymers that exhibit inverse temperature or lower critical solution temperature (LCST) phase behavior in aqueous solutions. These undergo a first-order phase transition from a soluble state into polymer-rich and water-rich phases upon heating above the cloud point (*i.e.*, transition temperature, T_t). That is, a polymer solution below the LCST is a clear and homogeneous solution, while cloudy due to polymer chains aggregation above the LCST. The understanding and the use of stimuli-responsive, in

particular temperature-sensitive, polymer materials have opened new potential applications, especially in the biomedical field, for therapeutic or diagnostic purposes *via* the elaboration of nanocarriers,⁵⁻⁷ or for the design of hydrogels for tissue engineering.^{8,9} Indeed, these can respond to subtle temperature differences, for example between cancerous and healthy cells,^{10, 11} and can also be used for hyperthermia-induced drug delivery purposes.¹²⁻¹⁵

Poly(*N*-isopropylacrylamide) (PNIPAm)^{16, 17} and poly(*N*-vinylcaprolactam) (PNVCL)^{18, 19} have been well studied and are probably the most popular thermoresponsive polymers,²⁰ partly because they both exhibit a LCST close to body temperature. However, a wide range of other thermoresponsive polymers have recently shown interesting properties. Among them, poly(2-oxazoline)s constitute an other synthetic class of polyamides for which small hydrophobic side-chains can lead to LCST behavior.^{21, 22} For example, poly(2-isopropyl-2-oxazoline)-*block*-poly(2-methyl-2-oxazoline) (PiPrOx-*b*-PMeOx) copolymers are able to form temporary or permanent micelles above the cloud point of the PiPrOx block based on its crystallization properties.²³ Amino-terminated random copolymer poly(ethylene glycol)-*co*-poly(propylene oxide) commercially known as Jeffamine and triblock poly(ethylene glycol)-*b*-poly(propylene oxide)-*b*-poly(ethylene glycol) (PEG-*b*-PPO-*b*-PEG) copolymers, named Poloxamer and commercially known as Pluronic were thoroughly investigated over the past several decades because of their thermoresponsive self-assembly properties in aqueous media.^{5, 24, 25} Moreover, poly(acrylate) and poly(methacrylate) bearing PEG chains also display a LCST depending on structural parameters (*i.e.*, nature of the polymerizable moiety, length of the PEG side chain or end-group of the PEG chain).²⁶⁻³⁰ Furthermore, grafting of hydrophilic side chains, usually tertiary amine,³¹ oligo(ethylene glycol),³²⁻³⁴ or poly[oligo(ethylene glycol) methacrylate],³⁵ on a synthetic hydrophobic polypeptide backbone, such as poly(γ -substituted *L*-glutamate), poly(*L*-

cysteine), or poly(*L*-lysine) allowed the design of biomimetic thermoresponsive materials.

A major limitation in the elaboration of this class of polymers is the need for extremely reproducible synthesis to preserve the precise temperature-triggered properties. To circumvent this drawback, another class of thermoresponsive polymers based on protein engineering has been developed, which demonstrates great promises for the preparation of adaptive and smart biomaterials.³⁶⁻³⁸ Indeed, in the past decade, recombinant protein-engineering techniques have allowed the development of precise recombinant polymers with exquisite control over their primary structure and their molecular weight.^{39, 40} Among them, elastin-like polypeptides (ELPs) are the most studied family of polypeptides that exhibit LCST in aqueous solution. ELPs share structural characteristics with intrinsically disordered proteins naturally found in the body, such as (tropo)elastin, at the origin of their name.^{41, 42} They are composed of repeating sequences of [-Val-Pro-Gly-*Xaa*-Gly-] pentapeptides, the guest residue *Xaa* being any amino acid except proline. The nature of the guest residue as well as the chain length encode for a precise transition temperature (T_t) at a given concentration.⁴³⁻⁴⁵ Recent contributions by our team have also demonstrated the possibility to easily tune the thermoresponsive properties of ELPs by chemoselective modifications at the guest residue position. In particular chemoselective alkylation^{46, 47} or oxidation⁴⁸ of methionine residues at the *Xaa* position have been used as an easy mean to modify the hydrophilicity and therefore LCST of specific ELP sequences. Regarding their distinctive properties, biocompatibility and biodegradability, these recombinant polypeptides have various applications, including the delivery of anticancer therapeutics to solid tumors⁴⁹ using self-assembled ELP-drug conjugates.^{50, 51}

In this context, a thorough understanding of the temperature-triggered self-assembly of ELPs is essential to take advantage of their unique properties. The thermoresponsiveness of ELPs has

been explained as the addition of two phenomena. The first one is a phase transition into polypeptide-rich and water-rich phases, as water becomes a poor solvent for the polypeptide chains upon heating above the T_t .⁵² Indeed, the transition is characterized by the loss of hydration of the polypeptide chains resulting in their aggregation.⁵³ The second one, also called folding process, is the formation of secondary structures, such as β -turns, due to the presence of regular prolyl-glycyl dipeptide sequence.^{52, 54}

The study of this thermoresponsive behavior in buffered or saline solutions mimicking physiological media is of major importance since such systems are intended to be used for biomedical purposes. It is well reported that salts cause generally significant, concentration-dependent, modification in T_t .^{55, 56} Amino acid side chains within ELP sequences being essentially uncharged and mainly apolar, this phenomenon cannot be attributed to direct ion binding to specific groups on the peptide chains nor a nonspecific electrostatic interaction. Rodríguez-Cabello and co-workers⁵⁷ assumed NaCl causes an increase in the solvent polarity, and that greater difference in polarity with respect to the hydrophobic moieties of the ELP causes more and more ordered structures of water surrounding the polymer chains leading to the folding process.

It was also demonstrated that, by increasing temperature above the critical micellar temperature (CMT), diblock ELPs of specific sizes gain enough amphiphilicity to organize into monodisperse micellar structures.⁵⁸⁻⁶¹ Due to the complex nature of ELPs, composed of both polar and nonpolar amino acids, these micelles have low surface tension at the core-corona interface and are considered as weak.⁶² To investigate the self-assembly phase of diblock ELPs, Garanger *et al.*⁶¹ studied a series of recombinant diblock ELPs with different hydrophobic block sizes ((VPGVG)₄₀₋₂₀₀-(VPG^A/G)₆₀) and determined the structural characteristics of the nanoparticles

obtained. In this study, micelles were found to be initially strongly hydrated and to continue to evolve upon heating above the CMT by compacting their core and gradually expelling water.

In the present work, we focus on the design and the temperature-triggered self-assembly of hybrid diblock copolypeptides. Only a few examples of self-assemblies based on polymer-ELP conjugates containing a thermoresponsive ELP block and a synthetic block have been reported in the literature. For example, van Hest and co-workers recently designed micellar nano-carriers of poly(ethylene glycol)-*b*-ELP conjugates.⁶³ Herein, we performed the synthesis of hybrid bioconjugates poly(*L*-glutamic acid)-*block*-elastin-like polypeptide (PGlu-*b*-ELP) by ring-opening polymerization of γ -benzyl-*L*-glutamate *N*-carboxyanhydride (γ -BLG NCA) and subsequent deprotection of the PBLG block. We investigated the self-assembly behavior of these thermoresponsive diblock copolypeptides in water and in phosphate-buffered saline (PBS) at the macroscopic and at the molecular scales by a large range of techniques, such as turbidimetry, dynamic and static light scattering, small-angle neutron scattering, ¹H NMR and circular dichroism.

Experimental section

Materials

All chemicals were purchased from Sigma-Aldrich and were used as received. γ -benzyl-*L*-glutamate *N*-carboxyanhydride (γ -BLG NCA) was purchased from Isochem and used without any purification. PBS corresponds to a phosphate-buffered saline (PBS) prepared in deionized water while PBS-D₂O was prepared in heavy water. In both cases, the composition is: NaCl 137 mM, KCl 2.7 mM, Na₂HPO₄ 8 mM, KH₂PO₄ 2 mM and pH = 7.2. The composition of the

phosphate buffer used is the following: (Na₂HPO₄ 8 mM, KH₂PO₄ 2 mM in H₂O, pH = 7.2).

Design of encoding gene, bioproduction, purification and isolation of recombinant ELP-M-40

The ELP-M-40 was recombinantly produced in *Escherichia Coli* bacteria as reported previously.⁴⁸ Its primary sequence is: MW[VPGVGVPGMG(VPGVG)₂]₁₀ and exact molar mass 17,035 g.mol⁻¹. The ¹H NMR spectrum of ELP was recorded in CDCl₃ (+ 15 % TFA) and carefully assigned (Figure S1).

Characterization techniques

¹H NMR

¹H NMR experiments were performed in CDCl₃ or DMSO-d₆ (with 15 % trifluoroacetic acid TFA) at 25 °C on a Bruker Avance I NMR spectrometer operating at 400 MHz and equipped with a Bruker multinuclear z-gradient direct probe head capable of producing gradients in the z direction with 53.5 G.cm⁻¹ strength. ¹H NMR spectra were recorded with an acquisition time of 4 sec, a relaxation delay of 2 sec and 64 scans. Thermoresponsive behavior was investigated by ¹H NMR in D₂O and D₂O-PBS at various temperatures.

Size exclusion chromatography (SEC)

The apparent molar masses and the dispersities of poly(γ -benzyl-L-glutamate)-*block*-ELP and ELP were determined by size exclusion chromatography (SEC) on a PL GPC50 integrated system from Agilent equipped with two KD-804 Shodex gel columns (300 × 8 mm) (exclusion limits from 4000 Da to 200 000 Da). The detector used in this determination is a refractive index detector (Jasco 1530-RI). Dimethylformamide (DMF) was used as eluent (0.8 mL.min⁻¹) at 50 °C in the presence of LiBr (1 g.L⁻¹) and the calibration used polystyrene (PS) as standard.

UV-Visible spectrometry

Transition temperatures (T_t) were determined by turbidimetry at 350 nm from 10 to 80 °C (then cooling from 80 to 10 °C) at 1 °C.min⁻¹ scan rate for various concentrations in deionized H₂O, PBS-H₂O, heavy water D₂O, PBS-D₂O and in phosphate buffer with various concentrations of NaCl (from 0 to 137 mM). The measurements were performed on two cycles (heating 1, cooling 1, heating 2, cooling 2) to verify the reversibility of the phenomenon. Data were collected on a Cary 100 UV-Visible spectrophotometer equipped with a multi-cell thermoelectric temperature controller from Agilent Technologies (Les Ulis, FR) and the solutions placed in 1 cm quartz cells. The T_t is defined as the temperature corresponding to the maximum of the derivative curve of the absorbance *versus* temperature, often also named inflection point.

Light scattering measurements

Mono-angle Dynamic Light Scattering (DLS) measurements were performed on a Malvern Instruments Zetasizer Nano ZS operating with a He-Ne laser source at the wavelength of 633 nm and a scattering angle of 90° at a constant position in the cuvette (constant scattering volume).

The autocorrelation functions ($g_1(t)$) were analyzed in terms of relaxation time distribution (τ) (Equation 1) and using the cumulants method.

$$g_1(t) = \int A_{(\tau)} \exp\left(-\frac{t}{\tau}\right) d\tau \quad \text{Equation 1}$$

Hydrodynamic radius (R_h) was determined from the Stokes-Einstein relation (Equation 2).

$$R_h = \frac{k_B T}{6\pi\eta_s D_0} \quad \text{Equation 2}$$

where D_0 is the diffusion coefficient, η_s is the viscosity of the solvent, T is the absolute temperature and k_B the Boltzmann constant.

Solutions were prepared in deionized H₂O and in PBS (pH = 7.2) at 1 g.L⁻¹. Three independent

measurements of fifteen 10 sec-runs were recorded and averaged. Temperature was raised from 20 to 80 °C and measurements were performed at each degree after a 2 min temperature equilibration time. The derived count rate (DCR) was defined as the mean scattered intensity normalized by the attenuation factor and used as arbitrary unit on the graph. This scattered intensity was plotted against temperature and the T_i is defined as the temperature corresponding to the point where the DCR starts to increase on this plot. The critical micellization temperature (CMT) is defined as the temperature corresponding to the point where the DCR starts to decrease.

Multi-angle Light Scattering measurements were performed using an ALV/CG6-8F goniometer, with a 35 mW red helium-neon linearly polarized laser ($\lambda = 632.8$ nm), an ALV/LSE-5004 multiple tau digital correlator and using a thermostated bath controller. The data were acquired with the ALV correlator software, the counting time was typically 15 sec for each scattering angle. Angles are ranging from 30° to 150° corresponding to scattering vectors q from $6.85 \times 10^{-3} \text{ nm}^{-1}$ to $2.55 \times 10^{-2} \text{ nm}^{-1}$. The autocorrelation functions ($g_1(t)$) were analyzed in terms of relaxation time distribution (τ) (Equation 1) and the hydrodynamic radius (R_h) was determined from the Stokes-Einstein relation (Equation 2). Light-scattering data were reduced using standard procedures. The solvent intensity was subtracted from that of the sample. Absolute calibration was performed against toluene.

The static light scattering allowed to calculate the radius of gyration (R_g) determined from a Zimm plot according to Equation 3:

$$\frac{1}{I} = \frac{1}{I_0} \times \left(1 + \frac{q^2 R_g^2}{3} \right) \quad \text{Equation 3}$$

Small-angle neutron scattering (SANS)

SANS experiments were performed at the Laboratoire Léon Brillouin (« ORPHÉE » reactor, CEA-CNRS Saclay, France) on the « PACE » spectrometer. The experimental scattering vector q ($q = (4 \pi / \lambda) \sin(\theta/2)$) range was $0.0025 < q \text{ (\AA}^{-1}\text{)} < 0.35$ and was covered by three configurations: (1) sample to detector distance $D = 4.7$ m and neutron wavelength $\lambda = 17 \text{ \AA}$, (2) $D = 3$ m and $\lambda = 6 \text{ \AA}$, and (3) $D = 1$ m $\lambda = 6 \text{ \AA}$. The samples were loaded into Hellma quartz cells with a 2 mm optical path length at a concentration of 1 g.L^{-1} in D_2O or $\text{D}_2\text{O-PBS}$ or in $\text{D}_2\text{O} + \text{NaOD}$ (pD = 9). The cells were placed in a sample changer, and the scattering for each sample was measured for about 2 hrs at various temperatures. The averaged spectra were corrected for empty cell, background noise, as well as for incoherent scattering. $I(q)$ is in absolute scale (cm^{-1}).

Modelling of SANS data

Analysis of the scattering intensity aims at obtaining the characteristic sizes, the shape and the interactions, represented by the form factor $P(q)$ and the structure factor $S(q)$. Classical expression of the scattering intensity per unit volume of particles is (Equation 4):

$$I(q) = n\Delta\rho^2V_{\text{part}}^2P(q)S(q) \quad \text{Equation 4}$$

where n is the number density of particles, $\Delta\rho$ is the difference in the scattering length density between the scattering species and the solvent, and V_{part} is the volume of scattering particles. The form factor describes the structure of particles and fulfills $P(q \rightarrow 0) = 1$ while the structure factor describes the interaction between particles. In dilute solution and consequently in the absence of interactions, $S(q) = 1$. Introducing the volume fraction $\Phi = nV_{\text{part}}$, Equation 4 becomes the Equation 5:

$$I(q) = \Phi\Delta\rho^2V_{\text{part}}P(q) \quad \text{Equation 5}$$

The data were fitted using the models available in the SaSview software (<http://www.sasview.org>).

Circular dichroism (CD)

Solutions of ELP and copolypeptide PGLu₂₃-*b*-ELP were characterized by UV CD analyzes at different temperatures below and above the T_i . CD spectra were recorded on a Jasco J-815 spectropolarimeter equipped with a FDP-425S Peltier temperature control unit in 1 mm quartz cells. Solutions in pure water and in PBS were prepared at 9 μ M of ELP block or at 14 μ M, for comparison with DLS data. Temperature-dependent CD scans were performed after a 2 min equilibration time at each temperature and at 1 $^{\circ}$ C. min^{-1} scan rate. Spectra were recorded at a scanning speed of 20 $\text{nm}\cdot\text{min}^{-1}$ from 260 nm to 180 nm with 0.1 nm resolution, 1 sec DIT and high sensitivity. CD spectra represent the average of two measurements. CD data are reported as mean residue ellipticity $[\theta]$ ($\text{deg}\cdot\text{cm}^2\cdot\text{dmol}^{-1}$) taking into account all the chromophores (peptides bonds) of diblock polypeptides.

Synthesis of poly(γ -benzyl-*L*-glutamate)-block-ELP diblock copolypeptides

Diblock copolypeptides poly(γ -benzyl-*L*-glutamate)-*block*-ELP were synthesized by ring opening polymerization (ROP) of γ -BLG NCA using ELP as macroinitiator. Various $[\text{monomers}]/[\text{macroinitiator}]$ molar ratios were used to obtain copolypeptides with different PBLG block lengths. For instance, PBLG₂₃-*b*-ELP was prepared as follows: γ -BLG NCA (94.2 mg, 3.58×10^{-1} mmol) was weighed in a glovebox under pure argon, introduced in a flame-dried schlenk, and dissolved in 2 mL of anhydrous DMF. The solution was stirred for 10 min, and the ELP-M-40 (244.0 g, 1.43×10^{-2} mmol) was added with a nitrogen purged syringe from a solution in anhydrous DMF (10 $\text{mg}\cdot\text{mL}^{-1}$, injected volume: 24.4 mL). The solution was stirred for one

week at 5 °C and precipitated in diethyl ether. Then the copolypeptide was isolated by successive centrifugations and dried under vacuum to afford a white powder. Yield: 285.0 mg (88 %). A copolypeptide with a total molecular weight of $22.0 \times 10^3 \text{ g}\cdot\text{mol}^{-1}$ corresponding to a degree of polymerization of 23 for the PBLG block was obtained.

Synthesis of poly(L-glutamic acid)-block-ELP diblock copolypeptides by acid deprotection of poly(γ -benzyl-L-glutamate)-block-ELP

The benzyl groups of the PBLG block were removed under mild acidic conditions as previously reported by Bonduelle and co-workers.⁶⁴ For instance, PBLG₂₃-*b*-ELP (160 mg, 1.65 mmol of BLG units) was dissolved in TFA (1.6 mL) and the reaction mixture was stirred at 0 °C (by using an ice bath). Then, anisole (0.32 mL) and methane sulfonic acid (MSA) (1.6 mL) were added to the solution and the reaction mixture was stirred for 20 min at 0 °C, and then 50 min at room temperature. The copolypeptide was finally precipitated twice in diethyl ether and collected by centrifugation. The precipitate was dissolved in DMSO and the resulting mixture was dialyzed against milliQwater (MWCO 15 kDa) for 4 days and freeze-dried to afford a white powder. Yield: 130 mg (90 %).

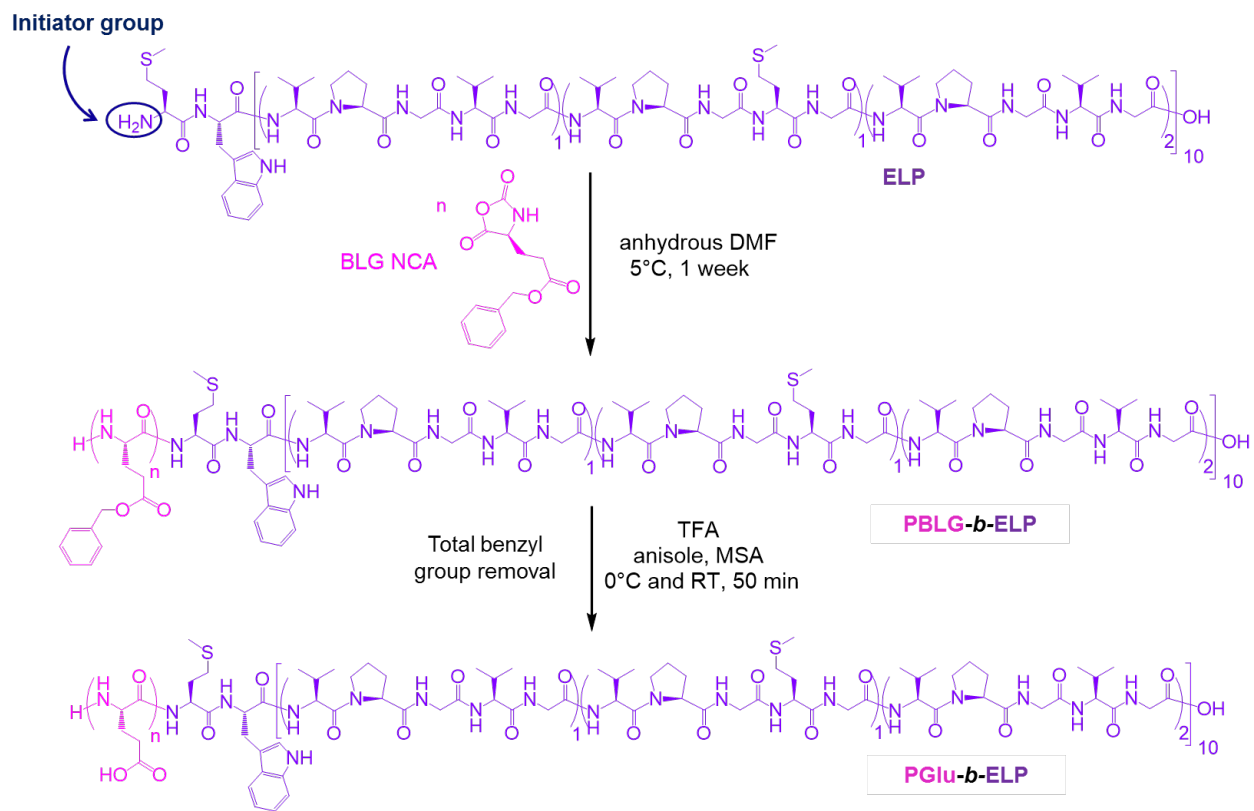
Results and discussion

Synthesis and characterization of hybrid PGLu-*b*-ELP diblock copolypeptides

The most convenient polymerization process to prepare synthetic poly(amino acid)s with high degrees of polymerization and excellent control over the dispersity is the ring-opening polymerization (ROP) of heterocycle α -amino acid *N*-carboxyanhydrides (NCAs) initiated by primary amine groups.⁶⁵⁻⁶⁷ As described in a previous work,⁶⁸ the primary amine group at the *N*-

terminal end of the ELP was advantageously used to initiate the polymerization of the γ -BLG NCA monomers. The ELP block contains a total of forty pentapeptide repeats according to the protein sequence MW[VPGVGVPGMG(VPGVG)₂]₁₀ corresponding to a molecular weight of 17,035 Da.⁴⁷ The ¹H NMR spectrum in CDCl₃ with 15 % trifluoroacetic acid (TFA, to compare with the spectra after polymerization) of the ELP was recorded and fully assigned (Figure S1 of the Supporting Informations) for subsequent comparison with PBLG-*b*-ELP and PGlu-*b*-ELP ¹H NMR spectra. The peak at 0.94 ppm attributed to the resonance of the methyl groups of the side chain of the 70 valine residues (420 ¹H total) was used for calibration.

The two-step method to synthesize poly(*L*-glutamic acid)-*b*-ELP (PGlu-*b*-ELP) diblock copolypeptides from poly(γ -benzyl-*L*-glutamate)-*block*-ELP (PBLG-*b*-ELP) used the initiation of the ROP of γ -BLG NCA by the *N*-terminal primary amine end group from the ELP, as represented in Scheme 1.



Scheme 1. Two-step synthesis of poly(*L*-glutamic acid)-*block*-ELP diblock copolypeptides.

In a first step, a series of hybrid copolypeptides with different PBLG block lengths was synthesized as previously reported.⁶⁸ Three PBLG-*b*-ELP diblock copolypeptides with degrees of polymerization (DPs) 23, 45 and 61 were obtained after complete conversions, according to the excellent agreement between the targeted and experimental DPs assessed by ¹H NMR (Figure S2, panel A). Analysis by size exclusion chromatography (SEC) in DMF (1 g.L⁻¹ LiBr at 50 °C with PS calibration and RI detector) (Figure S3) revealed apparent molar masses between 26,500 and 32,500 g.mol⁻¹, in agreement with those expected for the DPs obtained (between 22,000 and 30,400 g.mol⁻¹) and narrow dispersities ($D = 1.02 - 1.06$) that consequently confirmed the well-controlled behavior of the polymerization process.

The deprotection of the different PBLG-*b*-ELP diblock copolypeptides, in the second step, was achieved under acidic conditions, in TFA and in presence of methane sulfonic acid (MSA) and anisole. It has been established that this procedure did not alter the structure of the block copolymers.⁶⁴ The success of the reaction was confirmed by ¹H NMR analysis with the disappearance of the signal corresponding to the methylene group of the BLG units in α of the removed benzyl ring (Figure S2, panel B).

Three well-defined diblock copolypeptides poly(*L*-glutamic acid)-*b*-ELP (PGlu-*b*-ELP) with various lengths of PGlu block were therefore synthesized: PGlu₂₃-*b*-ELP, PGlu₄₅-*b*-ELP and PGlu₆₁-*b*-ELP. The molar masses of the PGlu blocks determined by ¹H NMR ranged from 3,000 to 7,900 g.mol⁻¹ corresponding to total molar masses between 20,000 and 24,900 g.mol⁻¹, as summarized in Table 1. The weight ratios of poly(*L*-glutamic acid) in the copolypeptides are 15, 25 and 32 % respectively, these values allowing to scan a range of ratios driving the self-assembly.

Table 1. Molecular characteristics of the copolypeptides poly(*L*-glutamic acid)-*block*-ELP

Diblock copolypeptides	Expected DP (PGlu)	DP (PGlu) (¹ H NMR)	\overline{M}_n PGlu ¹ H NMR (g.mol ⁻¹)	\overline{M}_n total ¹ H NMR (g.mol ⁻¹)	\overline{M}_n total SEC* (g.mol ⁻¹)	\overline{D} SEC*	Total yield (%)	<i>f</i> (%)**
PGlu ₂₃ - <i>b</i> -ELP	25	23	3,000	20,000	26,500	1.02	79	15
PGlu ₄₅ - <i>b</i> -ELP	45	45	5,800	22,800	29,600	1.02	82	25
PGlu ₆₁ - <i>b</i> -ELP	65	61	7,900	24,900	32,500	1.06	76	32

* SEC in DMF (0.8 mL.min⁻¹) at 50 °C in the presence of LiBr (1 g.L⁻¹) with RI detector, performed before the deprotection (*i.e.* for PBLG-*b*-ELP)

** *f* = mass fraction of poly(*L*-glutamic acid) in the copolypeptides.

Study of temperature responsiveness of PGlu-*b*-ELP diblock copolypeptides in pure water

The cumulative effects of chain length of the poly(*L*-glutamic acid) block and of the total molar mass increase on the thermoresponsive properties of the ELP block were evaluated by carrying out turbidimetry measurements at 350 nm in pure water at different concentrations of diblock copolypeptide (Figure 1, panel A for PGlu₂₃-*b*-ELP as example). The pH of the solutions was measured to be at 6.8, well above the pKa of glutamic acid units, that is about 5.5. For all the samples, a typical transition was observed. The reversible character of this phenomenon was verified by two cycles, with a hysteresis of -5 °C between the heating and cooling ramps under

our experimental conditions (Figure S4). Usually, a sharp increase in turbidity is reported to be an indicator of a phase transition from a soluble state to micron-sized aggregates.

Depending on sample concentration (25 μM to 1,250 μM corresponding to 0.43 $\text{g}\cdot\text{L}^{-1}$ to 21.3 $\text{g}\cdot\text{L}^{-1}$), the cloud point also called transition temperature (T_t , the temperature corresponding to the maximum of the derivative curve of the absorbance *versus* temperature) of the native ELP ranged from 26 to 32 $^{\circ}\text{C}$, in agreement with previous reports.⁴⁸ For PGlu-*b*-ELP diblock copolypeptides, T_t s were shifted to higher values as compared with the native ELP (Figure 1, panel B). Moreover, the longer the poly(*L*-glutamic acid) block, the higher the T_t . For instance, at 1 $\text{g}\cdot\text{L}^{-1}$, T_t obtained are 31 $^{\circ}\text{C}$ for the ELP, and 50 $^{\circ}\text{C}$, 58 $^{\circ}\text{C}$ and 64 $^{\circ}\text{C}$ for DPs of PGlu corresponding to 23, 45 and 61, respectively. The increase of the T_t with the PGlu block length was directly attributed to the increase of the overall hydrophilicity of the diblock copolypeptides in agreement with literature. Indeed, such an influence of overall hydrophilicity in thermoresponsive copolymers was previously demonstrated for ELP-based systems⁶⁹ as well as for synthetic copolymers such as PNIPAm⁷⁰ or poly[2-(dimethylamino)ethyl methacrylate].⁷¹ Moreover, a recent investigation on the thermoresponsiveness of series of resilin-like polypeptide-*block*-elastin-like polypeptide (RLP-*b*-ELP) showed the hydrophobic RLP block plays a role in modulating the T_t of the ELP block, longer RLP blocks lowering the T_t , thus demonstrating a clear mutual influence between the different blocks.⁷²

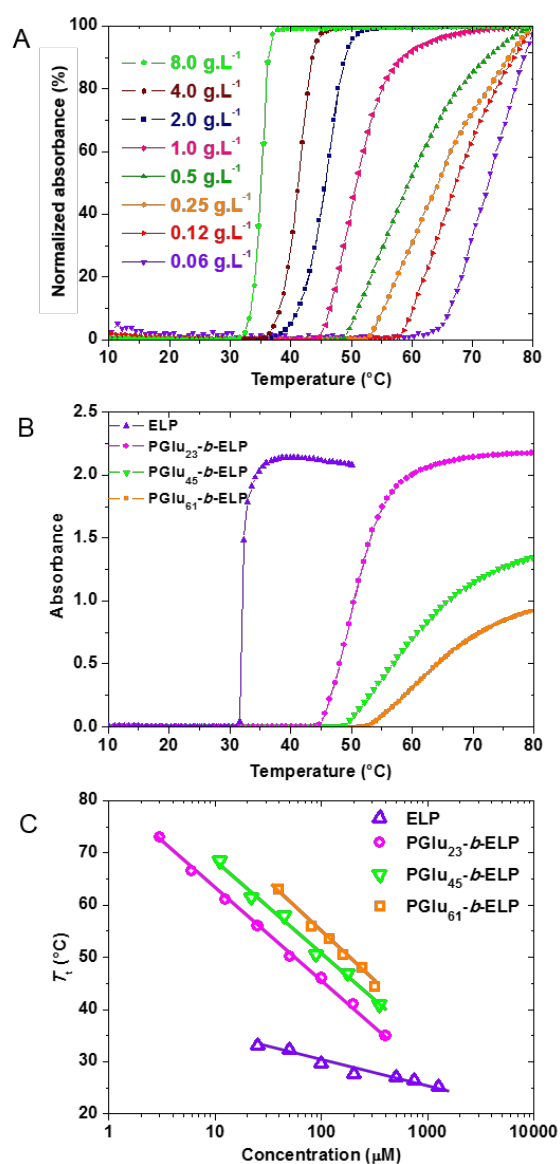


Figure 1. Turbidity assay in pure water. **(A)** Evolution of normalized absorbance (%) with temperature of solutions of PGLu₂₃-*b*-ELP at various concentrations. **(B)** Evolution of absolute absorbance at 350 nm with temperature of solutions of native ELP, PGLu₂₃-*b*-ELP, PGLu₄₅-*b*-ELP and PGLu₆₁-*b*-ELP at 1 g.L⁻¹. **(C)** T_t values of ELP, PGLu₂₃-*b*-ELP, PGLu₄₅-*b*-ELP and PGLu₆₁-*b*-ELP versus $\log_{10}(\text{concentration})$. Data fitted using Equation 7.

Figure 1, panel C shows that the presence of the poly(*L*-glutamic acid) block results in a significant increase of the concentration dependence as compared to the native ELP. The ELP sequence, chain length and concentration are primary parameters that modulate the T_t of ELPs. The effects of molecular weight and concentration are represented in the phase diagram described by Urry *et al.*⁴¹ However, in this diagram, the molecular weight effect was studied for a single concentration and for a precise pentapeptide sequence, resulting in an incomplete description of all the parameters influencing the thermoresponsive behavior. Because the ELP sequence is a key parameter that can be modified to modulate the T_t by introducing a particular guest residue,⁷³ Chilkoti and co-workers³⁹ elaborated an empirical model capable to predict the T_t of any new ELP construct designed for a specific application. They indeed established that the T_t is correlated to the molar concentration C with a logarithmic function (equation 6):

$$T_t = a \ln(C) + b \quad \text{Equation 6}$$

Their study revealed that the slope a is not only a function of ELP chain length, but also of peptide sequence. They deduced the following equality: $a = -k / L$ and established an empirical equation of three parameters that quantitatively predicts the T_t as a function of length and concentration for an ELP of a fixed composition. (Equation 7)

$$T_t = T_{t,c} + \frac{k}{L} \ln\left(\frac{C_c}{C}\right) \quad \text{Equation 7}$$

$T_{t,c}$ is the baseline T_t that is approached for a given sequence upon saturation of the concentration and chain length effects. The C_c represents a concentration at which the concentration effect is eliminated, and C is the concentration of ELP in solution. $T_{t,c}$ and C_c actually represent the critical values in the phase diagram, corresponding to the LCST. L is the number of pentapeptide units and can be correlated to the chain length. Mathematically, the constant k is defined as an interaction term acting as a modulator of the combined effects of chain length, concentration and

sequence.

In this work, we used the model from Chilkoti for our hybrid constructs PGlu-*b*-ELP to investigate the influence of the PGlu block length on the a parameter linking T_t and C .

We determined the a value (with $a = -k/L$ with $L = 40$, as 40 is the number of pentapeptide units both for the native ELP and the diblock copolypeptides PGlu-*b*-ELP) and consequently the constant k to study the different behaviors of the three diblock PGlu-*b*-ELP as compared to the native ELP.

The T_t values of the ELP and the three PGlu-*b*-ELP diblock copolypeptides were plotted *versus* $\log_{10}(\text{concentration})$ (Figure 1, panel C) and data were fitted using Equation 7. The values (slope, a and k) estimated from the linear fits are reported in Table 2. Obviously, in each sample, the result of the molar concentration calculation was the same considering only the ELP block or the diblock copolypeptides.

Table 2. Parameters describing the thermoresponsive behavior of native ELP and PGlu-*b*-ELP

	Polypeptide	<i>L</i> (Number of pentapeptides)	Slope* 2.30×<i>a</i>	<i>a</i> = -<i>k</i>/<i>L</i>	<i>k</i> (°C)	R²
Pure water	ELP	40	-1.996	-0.868	34.71	0.875
	PGlu ₂₃ - <i>b</i> -ELP	40	-7.578	-3.295	131.79	0.998
	PGlu ₄₅ - <i>b</i> -ELP	40	-7.927	-3.446	137.86	0.995
	PGlu ₆₁ - <i>b</i> -ELP	40	-9.061	-3.940	157.58	0.997
PBS	ELP	40	-3.803	-1.653	66.14	0.977
	PGlu ₂₃ - <i>b</i> -ELP	40	-6.451	-2.805	112.19	0.992
	PGlu ₄₅ - <i>b</i> -ELP	40	-5.058	-2.199	87.96	0.994
	PGlu ₆₁ - <i>b</i> -ELP	40	-5.843	-2.540	101.62	0.998

*taking account the following equality: $a \times \ln(C) = 2.30 \times a \times \log_{10}(C)$

All the data were properly fitted using this equation, allowing accurate estimations of the T_t of ELP as well as of the T_t of the diblock copolypeptides at specific concentrations (Figure 1, panel C). Importantly, we observed a steeper slope of the fits for the PGlu-*b*-ELP diblock copolypeptides than for the ELP. Indeed, the slope and k values for the ELP were -1.996 and 34.71 °C respectively, while the slope and k values, for the diblock copolypeptides, are ranged from -7.578 to -9.061 and from 131.79 °C to 157.58 °C, respectively, in an increased order of DPs (from 23 to 61). These results confirmed that the presence of the hydrophilic poly(*L*-

glutamic acid) block conferred a higher concentration dependence to T_t as compared to the native ELP. This result is comparable with observations by Meyer *et al.*³⁹ regarding the increase of the slope with decreasing ELP chain length, and by Petitdemange *et al.*⁴⁸ that chemically oxidized the methionine residues, which in both cases correlates with increased hydrophilicity. ~~The strengthening of the concentration dependence can be directly attributed to the increase of overall hydrophilicity as demonstrated previously with different ELPs with changes in the peptide sequence.~~^{39,48,74}

The thermoresponsive behavior of the P Glu_{23} -*b*-ELP diblock copolypeptide at 1 g.L⁻¹ in pure water was also studied by dynamic light scattering (DLS). The scattered light intensity in arbitrary units (a.u.) was plotted *versus* temperature, where an increase of scattered light identified the onset of aggregation (Figure S5). The plot revealed a typical one-step transition and the appearance of the aggregation phenomenon at 47 °C, similarly to our turbidity measurements. The continuous increase of the scattered light intensity with the temperature from the T_t value indicates that this phenomenon did not reach a steady state. The continuous increase of the scattered light intensity can be interpreted as a continuous dehydration of the ELP segment with temperature that increases the refractive index of the micro-aggregates and its scattering intensity, in agreement with previously reported data on Jeffamine-*b*-PGA systems.⁵

Small-angle neutron scattering (SANS) measurements was finally used for a fine characterization of the samples at the nanometric scale at various temperatures. Indeed, the configurations used allowed to probe a size range from 18 Å to 630 Å, while mono-angle DLS measurement at 90° provided a more global overview of the sample up to the micrometric scale and is very sensitive to the dispersity due to the presence of several size populations in the sample.

The native ELP and the three diblock copolypeptides, PGlu₂₃-*b*-ELP, PGlu₄₅-*b*-ELP and PGlu₆₁-*b*-ELP were therefore analyzed by SANS in D₂O. The shift on T_t values observed in H₂O and D₂O was previously quantified by UV-Visible spectrometry. T_{ts} in D₂O were found 5 °C below T_{ts} in H₂O (data shown for PGlu₂₃-*b*-ELP diblock copolypeptide only, Figure S6). This shift is easily explained by the lower bridge-bonding affinity of D₂O compared to H₂O.⁷⁴ Figure S7 shows SANS measurements on the PGlu₂₃-*b*-ELP in D₂O at 25 °C and at 65 °C. At 25 °C, below the T_t , the signal revealed a low scattered intensity with a slight upturn in the intermediate q range characteristic of chains in solution with few attractive interactions between individual diblock polypeptide chains. At 65 °C, well above the T_t , the scattered intensity was as low and did not show significant differences, excluding the presence of nanometric-sized self-assemblies, despite the macroscopic aggregation.

To conclude on this part, the three PGlu-*b*-ELP diblock copolypeptides underwent a sharp solubility transition in water from soluble chains to macroscopic aggregates. Despite the presence of the hydrophilic PGlu block and irrespective of its length (in the molar mass range investigated, corresponding to mass fractions of PGlu between 15 and 32 %), our observations confirmed the absence of stable nanoparticles. Nevertheless, it would be interesting to study the influence of a longer PGlu block on the organization of chains over the T_t . The fine-tuning of the thermoresponsive behavior of the ELP was however achieved by a convenient polymerization step, to introduce a controlled number of glutamic acid units at the ELP chain end.

Study of temperature responsiveness of PGlu_n-*b*-ELP diblock copolypeptides in phosphate-buffered saline (PBS)

Having characterized the aggregation behavior of this series of PGlu-*b*-ELP diblock

copolypeptides in pure water, we next investigated the thermoresponsive properties in a medium more compatible with biological studies. The thermoresponsive properties of the ELP and the different PGlu-*b*-ELP bioconjugates were therefore studied in phosphate-buffered saline (PBS) (NaCl 137 mM, KCl 2.7 mM, Na₂HPO₄ 8 mM, KH₂PO₄ 2 mM, pH = 7.2), as previously, by turbidity measurements at 350 nm (Figure 2).

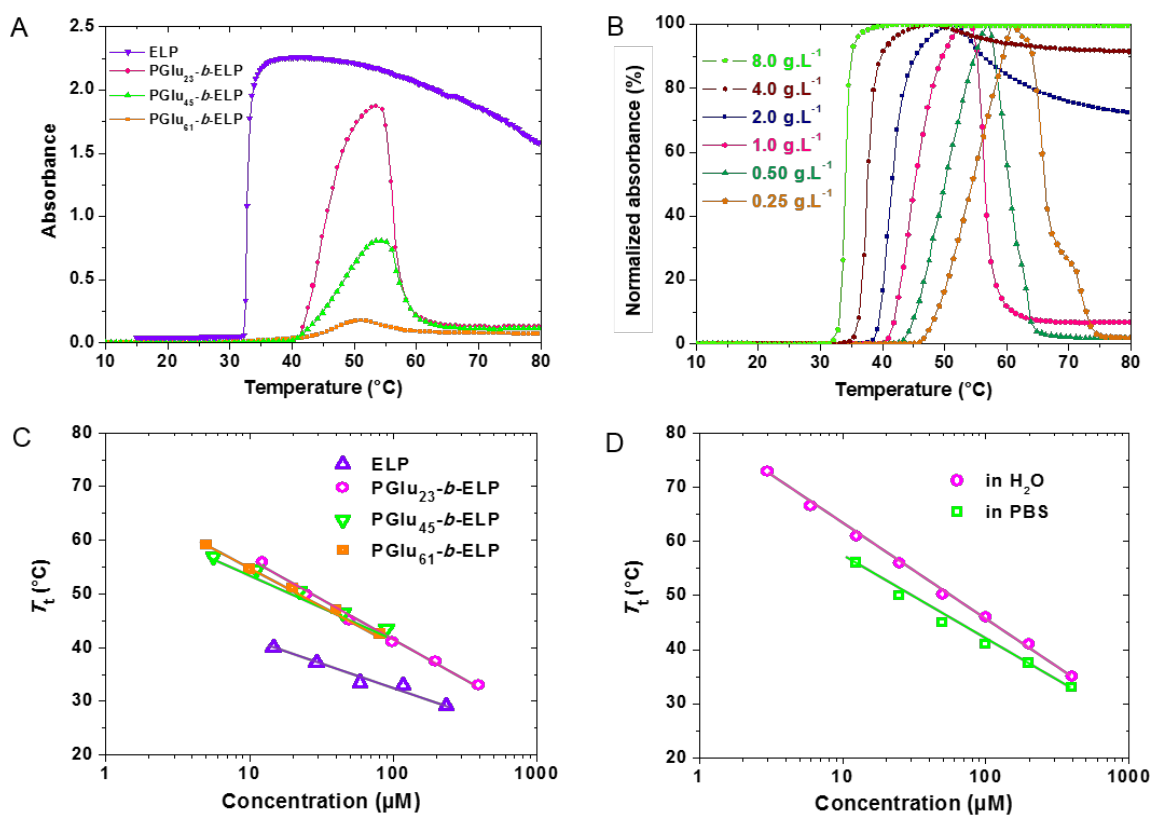


Figure 2. Turbidity assay in PBS. **(A)** Evolution of absolute absorbance with temperature of solution of native ELP, PGlu₂₃-*b*-ELP, PGlu₄₅-*b*-ELP, and PGlu₆₁-*b*-ELP at 1.g.L⁻¹. **(B)** Evolution of normalized absorbance (%) with temperature of solutions of PGlu₂₃-*b*-ELP at various concentrations. **(C)** T_t values of ELP, PGlu₂₃-*b*-ELP, PGlu₄₅-*b*-ELP and PGlu₆₁-*b*-ELP plotted *versus* \log_{10} (concentration) in PBS; data fitted using Equation 7. **(D)** T_t values of PGlu₂₃-*b*-ELP *versus* \log_{10} (concentration) in PBS and in pure water; data fitted using Equation 7.

In PBS, the native ELP showed the classical one-step transition with an almost twice-higher concentration dependence than in pure water. Indeed, in PBS, the slope and k values were -3.803 and 66.14 °C respectively; while they were -1.996 and 34.71 °C in pure water (Table 2 and Figure 3; panel A). Contrarily to our expectations, the presence of salts did not result in lower T_t over the entire concentration range. That may be due to relatively low NaCl concentration in PBS compare to saline solutions used in the literature.⁵⁷

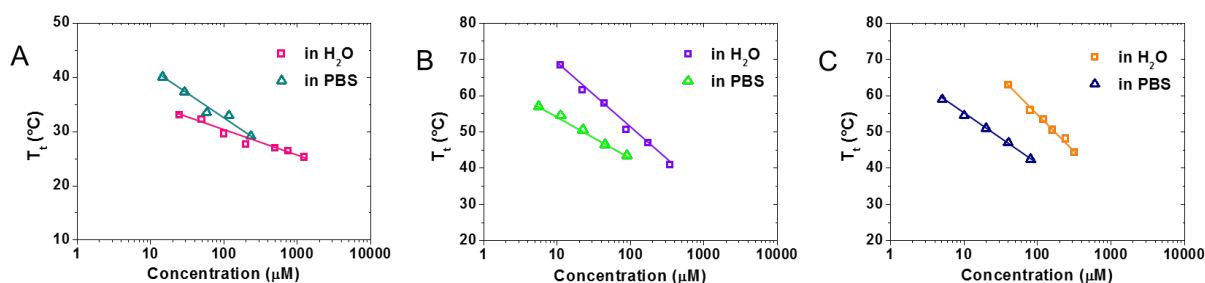


Figure 3. (A) T_t values of ELP *versus* $\log_{10}(\text{concentration})$ in pure water and in PBS. (B) T_t values of PGLu₄₅-b-ELP *versus* $\log_{10}(\text{concentration})$ in pure water and in PBS. (C) T_t values of PGLu₆₁-b-ELP *versus* $\log_{10}(\text{concentration})$ in pure water and in PBS.

More surprisingly the three PGLu-*b*-ELP copolymers showed a completely different behavior and exhibited four successive different regimes. Absorbance increased at a temperature corresponding to the T_t , and reached a maximum, almost at the same temperature for the three diblock copolymers (between 51 °C and 53 °C at $1 \text{ g}\cdot\text{L}^{-1}$) and decreased to finally return to almost zero value (Figure 2, panel A).

To get a better understanding of this four-phase behavior, we first investigated the influence of

salts on the T_t values, then explored the phenomenon leading to the turbidity drop. The T_t values of the PGlu₂₃-*b*-ELP copolyptide ranged from 33 to 56 °C depending on sample concentration (12.5 μM to 400 μM corresponding to 0.25 g.L⁻¹ to 8 g.L⁻¹) (Figure 2, panels B and C), while ranging from 36 to 61 °C in pure water at the same concentrations. The turbidity assay of the three PGlu-*b*-ELP diblock copolyptides at 1 g.L⁻¹ in PBS (Figure 4, panel A) and the plot of T_t values *versus* log₁₀(concentration) (Figure 2, panel C) highlighted that the T_t of the diblock copolyptides were very close from one another. The plot of T_t *versus* log₁₀(concentration) for PGlu₂₃-*b*-ELP in pure water and in PBS (Figure 2, panel D) showed that T_t in PBS was lower than in water for each concentration studied. This phenomenon was consistently observed for PGlu₄₅-*b*-ELP and PGlu₆₁-*b*-ELP diblock copolyptides but with a larger gap between the T_t values determined in PBS and in pure water as the PGlu block length increased (Figure 3 panels B and C). The slopes and k values in PBS obtained from the Equation 7 are reported in Table 2. Altogether, one can conclude from these measurements that the length of the PGlu block has limited influence on the T_t values in PBS in contrast to what is observed in pure water. This can be due to the screening of the negative charges of Glu units due to the increased salt concentration, which decreases its repulsion and hydrophilicity. For the three PGlu-*b*-ELP diblock copolyptides in PBS, when the temperature kept rising, the absorbance, after reaching a maximum around 52 °C ± 1 °C, decreased drastically (Figure 2, panels A and B) and reached a plateau. It has been optically verified that this phenomenon was not due to sedimentation in the bottom of the cell.

To investigate more thoroughly the effect of salts (NaCl, KCl), the turbidity assay was carried out for solutions of the PGlu₂₃-*b*-ELP diblock copolyptide at 1 g.L⁻¹ in phosphate buffer (Na₂HPO₄ 8 mM, KH₂PO₄ 2 mM, pH = 7.2) (pink curve in Figure S8). In such buffered solution,

the profile as well as the T_t value were similar to those in water (~ 51 °C). The presence of additional NaCl led to a decrease of T_t , from 50 °C at 1.37 mM to 45 °C at 137 mM (corresponding to NaCl concentration in PBS). The plot of the absorbance with increasing temperature showed that the four-phase behavior did not occur in phosphate buffer (without NaCl and KCl). The pH 7.2 was therefore not solely responsible for this phenomenon. In contrast, additional experiments showed that the decrease of absorbance became steeper with increasing NaCl concentration (Figure S8). We hypothesized a reorganization of the coacervates into a less absorbing suspension in the presence of salts due to screening effect between negatively charged Glu units.

The colloidal behavior of each PGlu-*b*-ELP diblock copolyptide was further studied by dynamic light scattering (DLS) for solutions at 1 g.L⁻¹ in PBS over a temperature range from 20 °C to 80 °C. The scattered light intensity in arbitrary unit (a.u.), the average hydrodynamic diameter (nm) and the polydispersity index (PDI) were plotted *versus* temperature, as shown in Figure 4 for PGlu₂₃-*b*-ELP and in Figure S9 for PGlu₄₅-*b*-ELP and PGlu₆₁-*b*-ELP. For PGlu₂₃-*b*-ELP diblock copolyptide, four successive regimes were clearly observed. The first regime, below the T_t , was characterized by a low scattered light intensity signal and high PDI values, reflecting the presence of faintly scattering single polypeptide chains and a few undefined aggregates that increased the average hydrodynamic radius observed. Above the T_t (39 °C) in the second regime, the scattered light intensity increased, highlighting the formation of sub-micrometric objects (with relatively low polydispersity, PDI < 0.2) with average hydrodynamic radii from 250 nm at 42 °C to 780 nm at 53 °C. The third regime, above 53 °C, showed a drastic decrease of both the scattered intensity and the hydrodynamic radius which dropped to 40 nm at 57 °C, highlighting a micellization phenomenon occurring at a critical micellization temperature

(CMT) of 53 °C. Both the size of the nanoparticles formed, and the scattered intensity are then stable above the CMT, suggesting that the system has reached a certain equilibrium. DLS measurements revealed clearly a similar four-phase thermoresponsive behavior for PGLu₄₅-*b*-ELP diblock copolyptide (Figure S9, panels A, B and C), with CMT at 57 °C and a hydrodynamic radius of 60 nm at the equilibrium. For the last diblock copolyptide, namely PGLu₆₁-*b*-ELP (Figure S9, panels D, E and F), DLS measurements did not allow to distinguish a clear behavior, even if the overall trend seems similar. It is reasonable to think that the longer the PGLu block, the less defined the transition due to the increase of copolymer hydrophilic fraction, and the lack of hydrophobicity to properly stabilize the micelles.

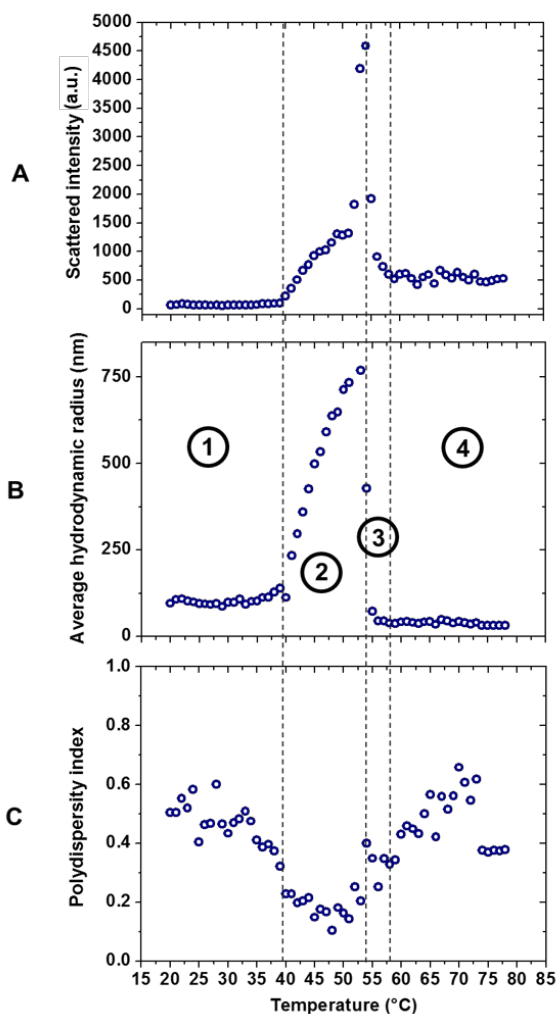


Figure 4. (A) Scattered light intensity, (B) average hydrodynamic radius and (C) polydispersity index *versus* temperature of a solution of PGlu₂₃-*b*-ELP diblock copolypeptide at 1 g.L⁻¹ in PBS (values obtained by DLS measurements at 90°).

Multi-angle dynamic and static light scattering measurements were subsequently used to determine with more accuracy the radius of gyration (R_g), the hydrodynamic radius (R_h) and the radius of gyration/hydrodynamic radius (R_g/R_h) ratio at various temperatures of PGlu₂₃-*b*-ELP in PBS at 1 g.L⁻¹. From 25 °C to 35 °C, a significant part of the correlation function resulted from

light scattered by polymer chains internal motions⁷⁵ and R_g/R_h ratios obtained ranged between 2.13 and 2.56 (Figure 5, panel A). At 40 °C and above this temperature, this ratio decreased drastically to reach values between 0.70 and 0.81, a typical signature of spherical compact form. Altogether turbidimetry, mono-angle and multi-angle DLS measurements showed an onset of self-assembly for PGlu₂₃-*b*-ELP at 40 °C. Above this temperature, DLS measurements showed monomodal hydrodynamic radius distributions (Figure 5, panel B). Corresponding R_h and PDI at each measured temperature are provided in the table of Figure 5, panel C. At 40 °C corresponding to the T_t , aggregates with an average R_h of 230 nm and 0.26 PDI are present. At 45 and 50 °C, R_h were 476 nm (PDI = 0.19) and 747 nm (PDI = 0.13) respectively and correspond to a transition phase during which large well-defined sub-micrometric particles were formed. At 55°C, the R_h decreased drastically down to 60 nm (PDI = 0.19), evidencing the micellization phenomenon. Finally, at 60 °C and above, micelles presented a monomodal hydrodynamic radius distribution centered on a R_h value of 40 nm with a PDI of 0.39. All these values were in good agreement to those obtained previously but did not allow to determine the nature of the sub-micrometric aggregates.

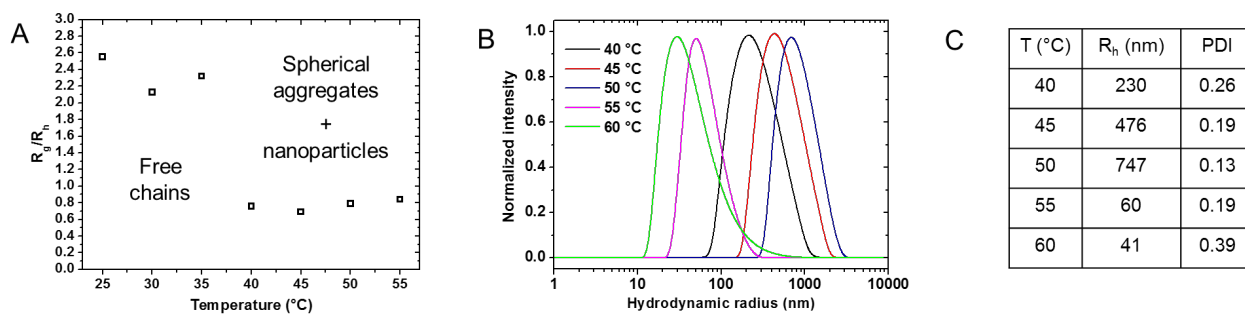


Figure 5. Light scattering results at various temperatures for PGlu₂₃-*b*-ELP in PBS at 1 g.L⁻¹. **(A)** R_g/R_h ratios obtained from multi-angle static and dynamic light scattering measurements, **(B)** hydrodynamic radius distribution at 90°, **(C)** table summarizing R_h and PDI values.

Higashi and co-workers⁷⁶ observed similar apparent transitions from free chains to aggregates to nanoparticles amino acid-based from block copolymers composed of *N*-acryloyl-Ala-methylester (NAAME) and *N*-acryloyl- β -Ala-methylester (Na- β -AME) in water. In their study, turbidimetry and ¹H NMR spectroscopy revealed formation of relatively loose-molecular packing at 17 °C, due to partial dehydration of polymer chains, and the formation of stable micellar structures between 30 and 39 °C. This phenomenon remained however unclear since no characterization technique invalidated or confirmed that the formation of micelles followed the disappearance of aggregates. Hoogenboom *et al.*⁷⁷ also reported comparable observations with diblock copolymers based on a poly(2-ethyl-2-oxazoline) and a thermoresponsive block consisting of a random copolymer of 2-ethyl-2-oxazoline and 2-*n*-propyl-2-oxazoline (PEtOx-*block*-P(EtOx-*stat*-PropOx)) in pure water. Even at temperatures significantly below the lower critical solution temperature (LCST) of the P(EtOx-*stat*-PropOx) block, copolymer unimers were found to coexist with a few aggregates. Upon heating, the systems exhibited a drastic increase of absorbance corresponding to the formation of large aggregates. When the temperature was further increased, solutions became visually clear again because of restructuration into smaller micelle-like structures. The authors assumed the first self-assembly behavior into large aggregates was due to the presence of a few swollen aggregates with unimers. In our case, due to the full reversibility of the phenomenon (free chains, aggregates, nanoparticles upon heating and nanoparticles, aggregates, free chains transitions upon cooling) (Figure S10), this hypothesis does not seem appropriate. Indeed, each regime appeared independently from the previous one, which evidence the intrinsic behavior of the system at a given temperature. In the same study, Hoogenboom and co-workers⁷⁷ supposed the formation of smaller micellar-like structures from

aggregates by contraction due to dehydration, and possibly also fragmentation which are hypotheses to consider in our case.

SANS measurements were therefore performed to gain better insight on the micellization phenomenon and to probe more precisely and quantitatively the structure of the nano-objects through appropriate models. The native ELP and the three diblock copolypeptides (PGlu₂₃-*b*-ELP, PGlu₄₅-*b*-ELP and PGlu₆₁-*b*-ELP) were studied in D₂O-PBS and also in D₂O + NaOD (to observe the effect of the pH/pD without salt) at a concentration of 1 g.L⁻¹ at increasing temperatures. The T_t in D₂O was beforehand determined by turbidimetry measurement in D₂O-PBS for each diblock copolypeptide (data shown for PGlu₂₃-*b*-ELP only, Figure S6). For the three diblock copolypeptides, a decrease by almost 9 °C was observed between the T_t value in PBS and the T_t value in D₂O-PBS. Figure 6, panel A shows the scattered intensity as a function of q for PGlu₂₃-*b*-ELP at 1 g.L⁻¹ in D₂O-PBS at various temperatures.

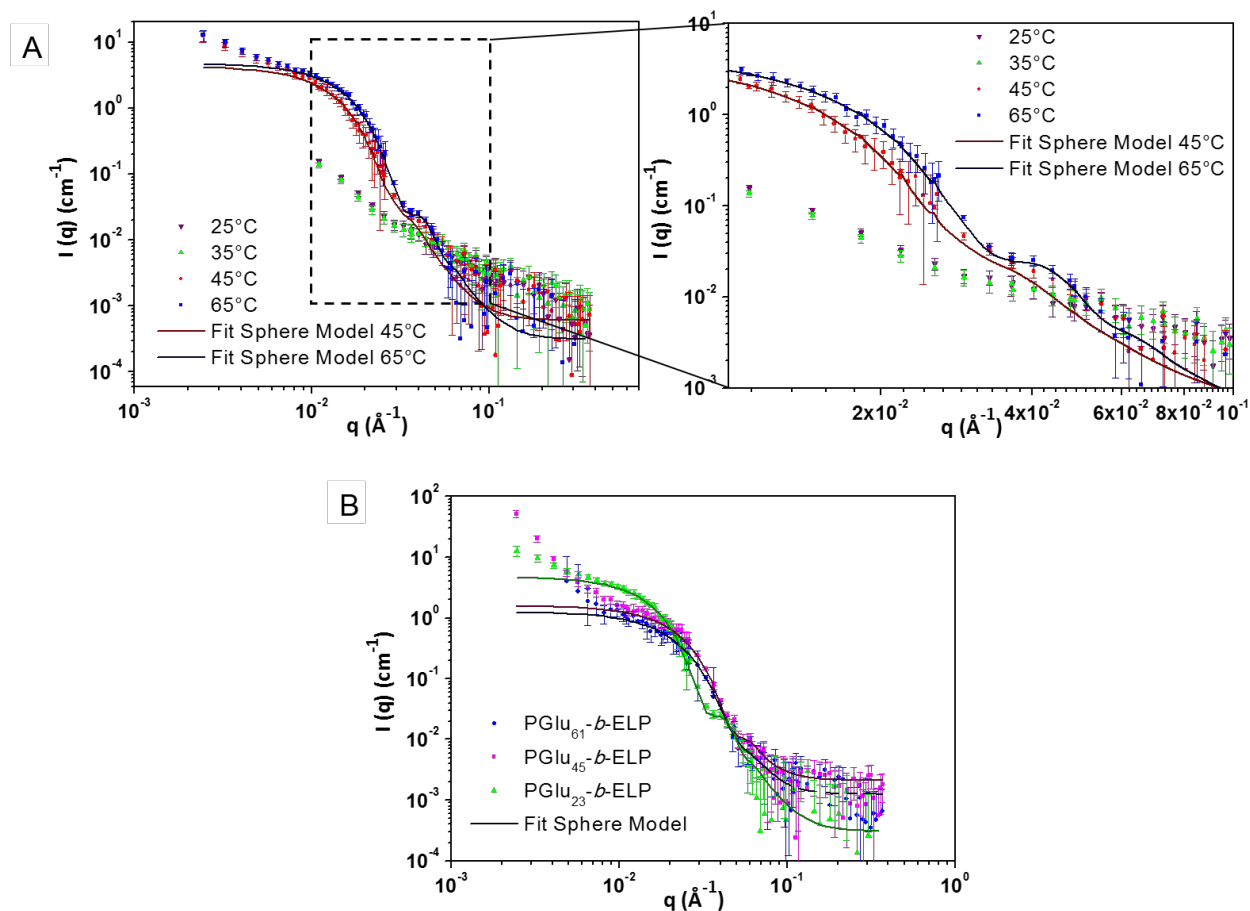


Figure 6. Small-angle neutron scattering of solutions of PGLu-*b*-ELP diblock copolypeptides prepared at 1 mg.mL⁻¹ in D₂O-PBS. **(A)** Scattering intensity as a function of q for PGLu₂₃-*b*-ELP at various temperatures; the solid line are the fitting curves obtained by using a polydisperse sphere model. **(B)** Scattering intensity as a function of q for PGLu₂₃-*b*-ELP, PGLu₄₅-*b*-ELP and PGLu₆₁-*b*-ELP at 65 °C ($> T_t$); the solid line are the fitting curves obtained by using a polydisperse sphere model.

Below the T_t ($T_t = 36$ °C in D₂O-PBS as shown in Figure S6), namely at 25 °C and at 35 °C, the low signal intensity evidenced the absence of nanometric aggregates. This absence of signal at 35 °C, just at the aggregation onset, proved that the first macroscopic aggregates in formation

were not composed of nano-assemblies, but can be considered as large and undefined coacervates. Moreover, the absence of signal at this temperature, despite a 2 hour-acquisition time, showed that the system did not evolve with time and depended solely on the temperature.

On the contrary, at 45 °C, well above the T_t , the drastic increase of the scattered intensity, by more than 1 order of magnitude and the appearance of a small oscillation at 0.03-0.05 Å⁻¹, is the hallmark of spherical nanoparticles. At 65 °C, the more pronounced oscillation clearly evidences that the nanoparticles are progressively better structured when temperature increases above the T_t . Based on the chemical structures of diblock copolypeptides, one can suggest that the nanoparticles are formed by an ELP core (more or less hydrated) surrounded by a corona of negatively charged PGlu chains. However, the contrast between the heavy water and the PGlu chains swollen in heavy water was too low to allow the monitoring of PGlu chains, the scattered signal being thus mainly due to the ELP core. Scattered intensity curves obtained at 45 °C and 65 °C (as well as at 55 °C and 70°C, data not shown) were fitted by a polydisperse sphere model using the SasView program. This Guinier model⁷⁸ describes a sphere of scattering length density (SLD) ρ_{sphere} and radius r_{sphere} (with a gaussian distribution on the radius) in a solvent of SLD ρ_{solvent} . In this case, there is only one contrast comparatively to the solvent, so, the mathematic expression is composed of 2 terms (Equation 8).

$$I(q) = \frac{\Phi}{V} [[V(\rho_{\text{solvent}} - \rho_{\text{sphere}})]^2 P_{\text{sphere}}(q)] \quad \text{Equation 8}$$

where V is the sphere volume and ρ_{solvent} the SLD of D₂O fixed at 6.4×10^{-6} Å⁻². This model provides the form factor, $P_{\text{sphere}}(q)$, for a monodisperse spherical particle with uniform SLD (Equation 9).

$$P_{sphere}(q) = \left[3 \frac{[\sin(qr_{sphere}) - qr_{sphere} \cos(qr_{sphere})]}{(qr_{sphere})^3} \right]^2 \quad \text{Equation 9}$$

The best fits using the polydisperse sphere model provided information about the structure of nanoparticles, such as the radius of their core (and the gaussian distribution of this radius σ_{sphere}), as well as their SLD (ρ_{sphere}) which is correlated to the degree of hydration. The values obtained for the three polypeptides at various temperatures above the T_t are summarized in Table 3. The fits are characterized by the ratio $khi2/NP_t$, the values obtained were low and comprised in a 0.74 - 2.02 range; indicating a good adequacy between the experimental curves and the fits. For the copolypeptide with the longer PGlu block, PGlu₆₁-*b*-ELP, the curve obtained at 45 °C was not fitted using a polydisperse sphere model due to the presence of free chains with the nanoparticles but using a sum of polydisperse sphere and the Debye form factors. Indeed, the Debye model is used to describe polymer chains in solution (as explained in Supporting Informations, Figure S11).

Table 3. Characteristics of the thermoresponsive nanoparticles of PGlu-*b*-ELP copolypeptides determined by SANS in D₂O-PBS.

Copolypeptide	T (°C)	Φ	Polydisperse Sphere Model					
			r _{sphere} (nm)	σ _{sphere}	ρ _{sphere} (Å ⁻²)	φ _{D₂O} (%)	N _{agg}	N ^{D₂O} / _{chain}
PGlu ₂₃ - <i>b</i> -ELP	45	0.00051	14.3	0.18	4.12×10 ⁻⁶	48.2	258	762
<i>T_t</i> = 36 °C	55	0.00057	13.3	0.15	3.95×10 ⁻⁶	44.3	223	653
	65	0.00060	13.6	0.12	3.87×10 ⁻⁶	42.5	246	606
	70	0.00060	13.8	0.10	3.86×10 ⁻⁶	42.3	258	600
PGlu ₄₅ - <i>b</i> -ELP	45	0.00051	8.0	0.36	4.47×10 ⁻⁶	56.1	33	1196
<i>T_t</i> = 37 °C	65	0.00052	8.9	0.17	3.64×10 ⁻⁶	37.3	56	555
PGlu ₆₁ - <i>b</i> -ELP	45	0.00039	6.6	0.32	4.53×10 ⁻⁶	57.5	17	1381
<i>T_t</i> = 38 °C	55	0.00055	7.0	0.37	4.17×10 ⁻⁶	49.3	24	965
	65	0.00050	8.3	0.19	3.92×10 ⁻⁶	43.6	44	790

The sphere fraction Φ was fitted and the values obtained are consistent with the fraction of ELP in the solution considering the presence of micrometric aggregates (as shown by DLS measurements). The scattered length density ρ_{sphere} was also fitted and evidenced the presence of D₂O molecules entrapped in the core, reducing the contrast with the solvent. Indeed, the theoretical neutron scattered length density of the ELP block is 2.0×10⁻⁶ Å⁻² and the values

determined here are in a 3.64×10^{-6} - 4.53×10^{-6} \AA^{-2} range. The fitting method therefore allowed us to calculate the volume fraction of D_2O molecules (φ_{D_2O}) in the core of spherical nanoaggregates by the following equation:

$$\varphi_{D_2O} = (\rho_{\text{sphere}} - \rho_{\text{ELP}_{\text{theo}}}) / (\rho_{D_2O} - \rho_{\text{ELP}_{\text{theo}}}) \quad \text{Equation 10}$$

The aggregation number N_{agg} , defined as the number of chains per sphere, was then estimated using Equation 11:

$$N_{\text{agg}} = \frac{N_A d}{M_n} (1 - \varphi_{D_2O}) \left(\frac{4\pi r_{\text{sphere}}^3}{3} \right) \quad \text{Equation 11}$$

where $d = 1.35 \text{ g.cm}^{-3}$ is the mass density as reported for proteins in the crystalline state,⁷⁹ \overline{M}_n the molar mass of the diblock copolypeptides determined by ^1H NMR, r_{sphere} the radius of the core of the nanoparticles from the fits and N_A the Avogadro number. The φ_{D_2O} and N_{agg} values are summarized in Table 3. To determine the degree of hydration of the polypeptide chains within the nanoparticles, we estimated the number of D_2O molecules per chain from this volume fraction φ_{D_2O} , the aggregation number N_{agg} and the molecular volume, $v = 30 \text{ \AA}^3$ corresponding to one D_2O molecule:

$$N_{\text{chain}}^{D_2O} = \frac{\varphi_{D_2O}}{N_{\text{agg}} \cdot v_{D_2O}} \left(\frac{4\pi r_{\text{sphere}}^3}{3} \right) \quad \text{Equation 12}$$

r_{sphere} and aggregation numbers N_{agg} values for the three copolypeptides deduced from the fits were compared depending on the DP of PGlu chains at each temperature studied (Table 3). The values obtained for PGlu₂₃-*b*-ELP, the copolypeptide with the shortest PGlu block length, suggested that the radius and N_{agg} were almost constant from the formation of micelles and when the temperature further increased. Equation 12 allowed to deduce the confinement of about 760

D₂O molecules per chain at 45 °C. At 65 °C and 70 °C, the degree of hydration decreased to $N_{/chain}^{D_2O} \sim 600$ D₂O molecules, indicating a denser state of aggregation. Altogether, these results revealed that once the CMT was reached, no additional copolypeptides chains were incorporated (N_{agg} constant over the temperature range studied), but nanoparticles continued to evolve, in a “densification” phase by expelling water until they reach an equilibrium (at 65 °C). These observations are in agreement with previous findings about the temperature-triggered self-assembly behavior of diblock ELPs with different hydrophobic block sizes.⁶¹ However, for the diblock copolypeptides with the highest PGlu block lengths, the radius and N_{agg} continued to increase with temperature from $r_{sphere} = 8.0$ nm and $N_{agg} = 33$ at 45 °C to $r_{sphere} = 8.9$ nm and $N_{agg} = 56$ at 65 °C for PGlu₄₅-*b*-ELP and from $r_{sphere} = 6.6$ nm and $N_{agg} = 17$ at 45 °C to $r_{sphere} = 8.3$ nm and $N_{agg} = 44$ at 65 °C for PGlu₆₁-*b*-ELP. In the same time, the temperature increase led to a dehydration of the core (Table 3) highlighted by the decrease of the hydration level and the decrease of D₂O molecules number. This observation demonstrated that the “self-assembly” phase and the “densification” phase have occurred simultaneously when the PGlu block was longer. Finally, Figure S12 shows the scattered intensity of the PGlu₂₃-*b*-ELP as a function of q in D₂O and in D₂O with 1 eq of NaOD / Glu unit (allowing to reach a pD = 9) at 65 °C ($> T_t$). In each case, the signal revealed low scattered intensity. This confirmed that an increase of pH is not solely responsible for the formation of nano-objects.

Proposed self-assembly scenario for PGlu-b-ELP diblock copolypeptides

To summarize, DLS, SLS, and SANS measurements revealed the particular self-assembly behavior of PGlu-*b*-ELP diblock copolypeptides in PBS. Below the T_t , diblock copolypeptides were soluble and formed, above the T_t , monodisperse sub-microscopic aggregates, which

spontaneously evolved into nano-objects at the CMT. CMT seemed dependent on the ELP thermoresponsive block driving the self-assembly, as previously demonstrated by MacKay and co-workers for diblock ELPs.⁸⁰ When increasing the temperature above the CMT, small-angle neutron scattering measurements evidenced a slight increase of the aggregation number of polypeptide chains (except for PGlu₂₃-*b*-ELP) and a clear dehydration of the core. These phenomena compensated each other, allowing the core radii to remain constant. These experiments confirmed that even well above the CMT, ELP-based diblocks need to gain sufficient amphiphilicity to undergo stable self-assembly into spherical micelles.^{59, 81} A comparison of the R_h obtained by DLS measurements with the core radii r_{sphere} deduced from the SANS curves highlighted a gap corresponding to the PGlu hydrophilic corona of thickness δ_{corona} . For each diblock copolypeptides, we deduced $\delta_{\text{corona}} \gg r_{\text{sphere}}$, corresponding to the formation a star-like micellar structure.⁸² Our investigations revealed the formation of stable micelles for low hydrophilic weight fractions of 15 % while the screening experiments performed by Chilkoti and co-workers on 10 non-charged diblock ELPs revealed that only hydrophilic weight ratios between 33 % and 66 % allowed the micelle formation.⁵⁹ This observation showed that the non-charged and charged systems behave very differently and do not follow the same general rules. Indeed, the association equilibrium and the structure of “polyelectrolyte micelles” formed by block copolymers with charged soluble block are governed by the competition between hydrophobic attraction of insoluble blocks to form the core and the Coulomb repulsion between charged repetitive units in the corona. ~~The latter interaction is strongly mediated by counterions, which are always present but in larger amount in saline solutions. Borisov and Zhulina applied a scaling model to describe a micellization of charged-neutral diblock copolymers in salt free medium. The~~ Generally, the N_{agg} appears to be a strongly

decreasing function of the degree of polymerization of charged block. As a result, polyelectrolyte star-like micelles are expected to be marginally stable in salt-free solutions that corresponds to the classical two-phase behavior observed in pure water for our system. Dan and Tirrell⁸³ investigated the micellization of charged-neutral diblock copolymers in dilute salt solution. Micellar phase properties were predicted to be quasi-similar to those of neutral amphiphilic copolymers as salts ensure screening effect between charged moieties, thus the behavior of the corona is dominated by steric repulsions between the chains.

To complete these observations, the mobility of the native ELP chains (data not shown) and of PGLu₂₃-*b*-ELP diblock copolypeptide chains at the molecular scale was studied by ¹H NMR at various temperatures in D₂O and in D₂O-PBS at 1 g.L⁻¹ (Figure S13, panel A and Figure 7, panel A respectively). The modification in the chemical shift signal corresponding to the proton from non-completely deuterated water (named HDO) with the increase of temperature is well known and described in the literature.⁸⁴ Regarding the native ELP, ¹H NMR spectra showed the quasi-total disappearance of the signals from 30 °C in D₂O and in D₂O-PBS, highlighting a significant loss of mobility of the chains, due to their confinement into compact aggregates. On the contrary, PGLu₂₃-*b*-ELP diblock copolypeptide showed a slightly different behavior. In D₂O and in D₂O-PBS, below the *T*_t value, the entire copolypeptide chains were found fully hydrated and flexible, evidenced by well-resolved and sharp ¹H resonance peaks of the copolypeptides. Above the *T*_t, in D₂O and in D₂O-PBS, the intensity of resonance peaks decreased gradually, became weak and poorly resolved as a consequence of a decrease of the mobility of the chains indicating their confinement within the aggregates but demonstrated an incomplete dehydration even at the highest temperature studied (61 °C).

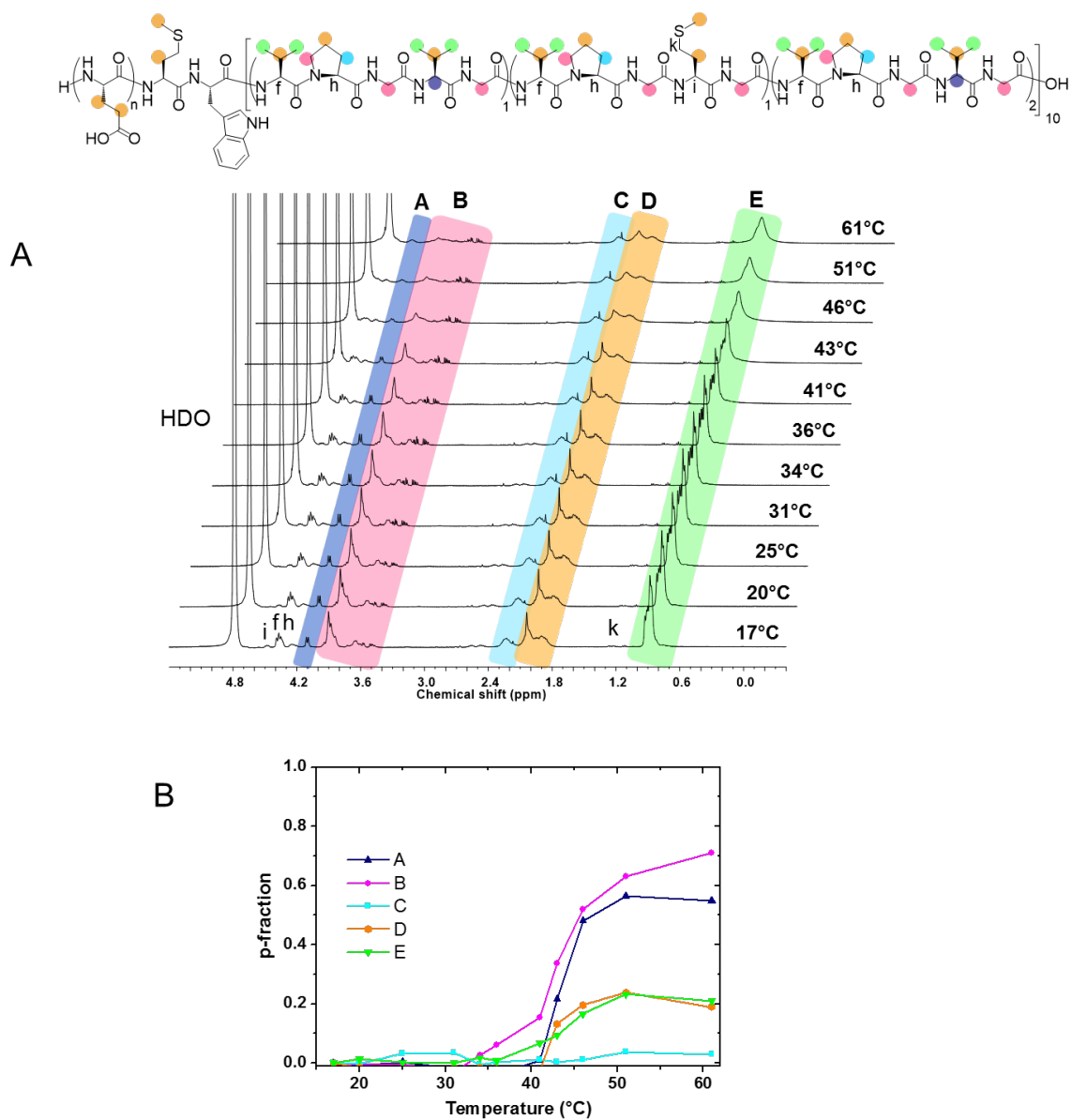


Figure 7. (A) ^1H NMR spectra of PGLu₂₃-*b*-ELP in D₂O-PBS (1 g.L⁻¹) at various temperatures.

(B) Phase separation fraction p from ^1H NMR signals A, B, C, D and E plotted as a function of the temperature.

Similar phenomena have been described in detail for aqueous solutions of PNIPAm.⁸⁵ Moreover, the residual signals observed at 61 °C were found more intense in D₂O-PBS than in D₂O. This observation implies that the copolypeptide chains have still possessed significant mobility in

PBS beyond their T_i .

To characterize more quantitatively the changes occurring during the heating process, the p values, defined as the fraction of phase-separated units in globular structures were calculated from the integrated intensity of the resonance peaks A, B, C, D and E in ^1H NMR spectra (Figure 7, panel A) using Equation 13^{86, 87}:

$$p = 1 - I(T)/I(T_0) \quad \text{Equation 13}$$

where $I(T)$ is the integrated intensity of a given signal in the spectrum at the temperature T and $I(T_0)$ is the integrated intensity of the same signal below the T_i (at 17 °C). In the Figure S13, panel B and Figure 7, panel B for P Glu_{23} -*b*-ELP in D_2O and D_2O -PBS respectively, the p -fractions were plotted as a function of temperature. In D_2O (Figure S13, panel B), the temperature dependences of the p -fraction of protons A ($\text{H}\alpha$ of Val as guest residue) and B ($\text{H}\alpha$ Gly and $\text{H}\delta$ Pro) showed an important increase starting at 29 °C to reach values around 0.70. In the same way, the p -fractions for the signals D ($\text{H}\beta$ and $\text{H}\epsilon$ Met, $\text{H}\beta$ Val, $\text{H}\gamma$ Pro and $\text{H}\beta$ and $\text{H}\gamma$ Glu) and E ($\text{H}\gamma$ Val) increased to 0.40 and 0.30 respectively. Moreover, the p -value attributed to the signal C, the only one corresponding to proline units solely ($\text{H}\beta$ Pro) increased radically from 29 °C to reach 0.80 at 40 °C. In D_2O -PBS (Figure 7, panel B), the temperature dependences of the p -fraction of protons A and B showed an increase starting at higher temperature (at 41 °C and 31 °C respectively) as compared in D_2O alone, to reach p -values of 0.55 and 0.70 respectively. Moreover, the traces for the signals D and E increased only to 0.20. Interestingly and contrary to the observations in D_2O , the signal C did not increase at all despite the increase in temperature.

Surprisingly, in D_2O , p -value increase was observed at lower temperature than in D_2O -PBS while the opposite seemed to be observed at the macroscopic scale, indicating that the two

phenomena are different, and both participate in the global thermoresponsiveness. The various p values showed, in D₂O as well as in D₂O-PBS, a similar confinement of Val as guest residue and of Gly, and a slightly better mobility of the Met and the Val units in D₂O-PBS. Moreover, a sharp and important increase of p-value corresponding to the dehydration of proline units was observed in D₂O, confirming the important role of this amino acid residue in the folding process. On the contrary, in PBS, the p-value corresponding to the proline residues remained almost at zero, indicator of a lack of ordered structures involving particularly this residue, in the aggregation phase. Recently, Yingling and co-workers⁸⁸ showed the role of proline units by investigating the effect of temperature on the structure, dynamics and association of (VPGVG)₁₈ in aqueous solution using atomistic molecular dynamics simulations. Their results concluded that the thermoresponsive behavior of this ELP is a collective phenomenon between the abrupt modifications of hydration properties around the polypeptide chain (competition between peptide-peptide and peptide-water interactions) and the gradual changes in single polypeptide structure. More precisely, increasing the temperature leads to a change in the hydrophobicity of the ELP by exposing the hydrophobic valine-side chains to the solvent and by hiding the proline residues, which may explain such a difference between the p-values obtained for the proline units. Our observations coupled with the results obtained by Yingling showed that PGlu₂₃-*b*-ELP has a tendency to undergo a folding process more in salt-free medium than in PBS.

For a better understanding of the self-assembly process at the molecular level, solutions of native ELP and PGlu₂₃-*b*-ELP in deionized water and PBS were characterized by UV circular dichroism (CD) at different temperatures (Figure 8). CD is a characterization technique involving circularly polarized light, that is, the differential absorption of left- and right-handed light, allowing the investigation of secondary structures of proteins. pH of solutions in water (pH

= 6.8) and in PBS (pH = 7.2) were not compatible with the formation of α -helix structures from the PGlu block (usually observed for PGlu at acidic pH below the pKa about 5.5) due to the deprotonation of the acid moieties, as evidenced by the absence of minima at 208 and 222 nm.⁸⁹

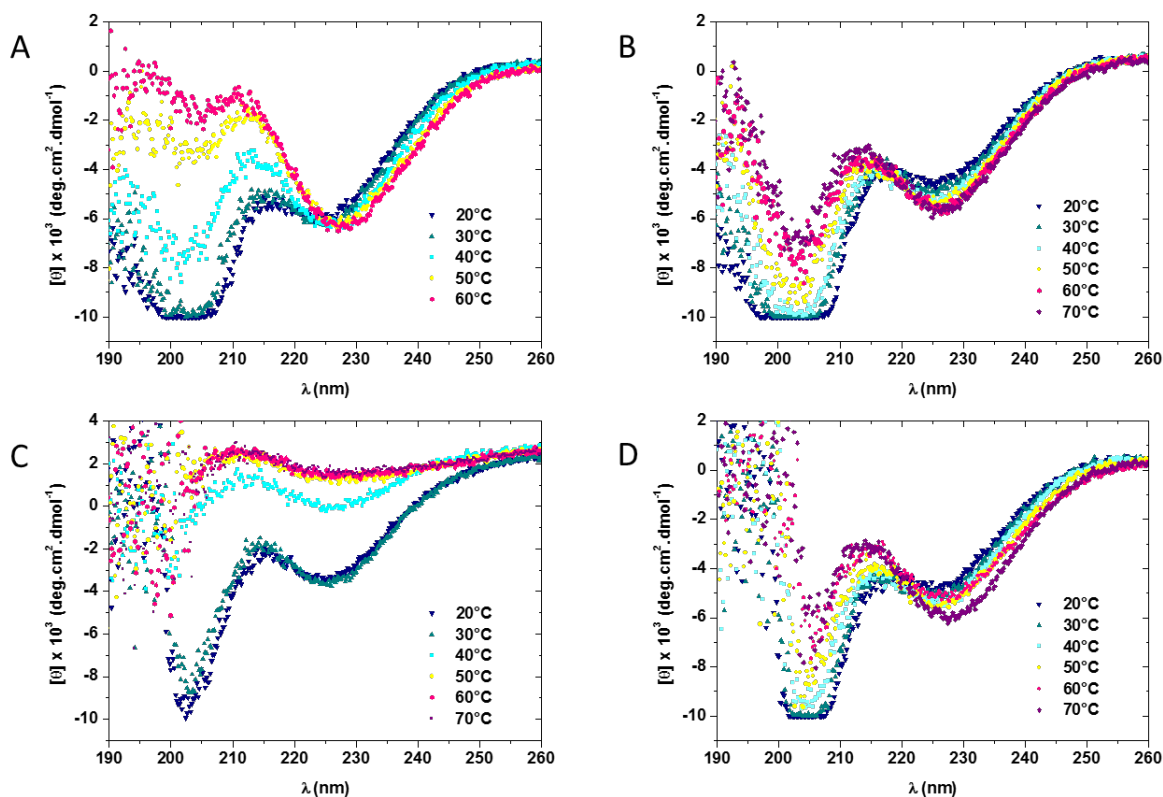


Figure 8. Circular dichroism spectra of ELP (A) and PGlu₂₃-b-ELP (B) in pure water and circular dichroism spectra of ELP (C) and PGlu₂₃-b-ELP (D) in PBS.

CD spectra of native ELP (Figure 8, panel A) and PGlu₂₃-b-ELP diblock copolyptide (Figure 8, panel B) in pure water at 20 °C showed a minimum at 195-205 nm corresponding to disordered peptides. The positive signal between 210 and 215 nm are classically attributed to more ordered secondary structures named type II β -turns.⁹⁰⁻⁹² The negative ellipticity peak

around 225 nm often observed for ELP, corresponds to other regular secondary structures, since ELPs CD spectrum is described as a combination of unordered, β -turns but also β -strand and helix conformations, which is largely consistent with the reported secondary structure of tropoelastin (3% helix, 41% β -strand, 21% β -turn, and 33% unordered).⁹³ This suggests that this ELP, adopted already a local ordered conformation even at low temperature. CD spectra of ELP in water acquired at various temperatures showed the gradual disappearance of unordered phase to the benefit of the formation of type II β -turns, as confirmed by $[\theta]$ values at 205 nm and 215 nm plotted as a function of the temperature (Figure S14, panel A). Indeed, as already shown by MacKay and co-workers,⁸⁰ ELPs have the propensity to form secondary structures as they undergo their phase transition. However, the signal at 225 nm stayed almost constant upon the temperature raised. A quasi-similar behavior was observed for PGlu₂₃-*b*-ELP diblock copolypeptide in water (Figure 8, panel B and Figure S14, panel B), nevertheless, despite a reduction of the signal at 195-205 nm, it remained significant, even at 70 °C, indicating the co-existence of an unordered phase with type II β -turns. This result showed that the presence of the PGlu had a tendency to decrease the capacity of ELP block to form ordered structures in pure water. These observations can be correlated with the presence of persistent signals from PGlu₂₃-*b*-ELP observed by ¹H NMR in D₂O during the formation of more ordered structures, contrarily to native ELP for which the signals disappeared. On the contrary, the CD spectrum obtained for ELP in PBS (Figure 8, panel C) and the plots of $[\theta]$ values with the temperature (Figure S14, panel C) showed an abrupt and important reduction of the signal at 205 nm between 30 °C and 40 °C ($T_t = 35$ °C at 9 μ M) as well as a sharp increase of the signals at 215 nm corresponding to type II β -turns and the disappearance of the negative signal at 225 nm. These result confirmed the assumptions of Rodriguez-Cabello and co-workers⁵⁷ who supposed that NaCl, has a strong

salting-out effect, and causes more ordered structures. Indeed, NaCl acts a structure-maker for water molecules and consequently strengthens the intramolecular interactions.

Finally, the CD spectrum of the PGlu₂₃-*b*-ELP in PBS (Figure 8, panel D) and the plots of the signals intensity as a function of the temperature (Figure S14, panel D) revealed the sharp decrease of the proportion of unordered phase and the formation of type II β -turns. Moreover, a progressive increase of the signal at 225 from 20 to 50 °C and a slight decrease at 60 °C followed by an increase at 70 °C were observed. At this concentration (9 μ M), this decrease of the signal between 50 °C and 60 °C was correlated with the T_t , thus these curves showed sudden variations into the secondary structure during the self-assembly process.

The secondary structure of ELPs has been a point of debate and several research groups have investigated the secondary structures of ELPs below and above their T_t . Most of them agree on the formation of type II β -turns resulting from the presence of prolyl-glycyl dipeptides and stabilized by intramolecular hydrogen bonds between the first and fourth residues of the pentapeptide (respectively valine and the guest residue valine or methionine in our case).^{56, 94, 95} A description of the secondary structure in the folded state has been determined by the work of Urry for the [-Val-Pro-Gly-Val-Gly-] repeating sequence. Their model indicated that the polypeptide chains change conformation from a random coil below T_t to type II β -turns that arrange into helical β -spirals above T_t , while simultaneously releasing hydrating water molecules.^{56, 96} This structure is stabilized by intra-spiral, inter-spiral and inter-turn hydrophobic contacts.⁹⁷ Nevertheless, a solid-state NMR study as well as computer simulations have also been employed to explore the thermoresponsive mechanism of poly(VPGVG) in aqueous solution suggested that Urry's model missed the significant formation of distorted β -strand structures.^{19, 98} Moreover, a study of (GVGV₆)₆ by Gross *et al.*⁹⁹ suggested that the polypeptide

could adopt a β -sheet structure instead of a β -spiral in the folded state. Some other teams postulated about the formation of polyproline II (PPII) structure, a relatively open left-handed helical structure caused by the presence of proline units at regular intervals. PPII has no internal hydrogen bonding, as opposed to the more common helical secondary structure, α -helix. It was often confused with unordered, disordered, irregular, unstructured conformations because it is neither α -helical nor β -sheet.¹⁰⁰ Clearly, there is considerable disagreement about the nature and degree of the structural changes and ordering upon heating of ELPs.

For a better understanding of the relationship between the various modifications occurring into the secondary structure and the self-assembly process depending on the temperature, we plotted the scattered light intensity values (obtained by DLS at 90°) and more accurately the $[\theta]$ values from CD signals at 205 nm and 225 nm as a function of temperature, obtained for a solution of P Glu_{23} -*b*-ELP diblock copolypeptides at 14 μM in PBS (Figure 9).

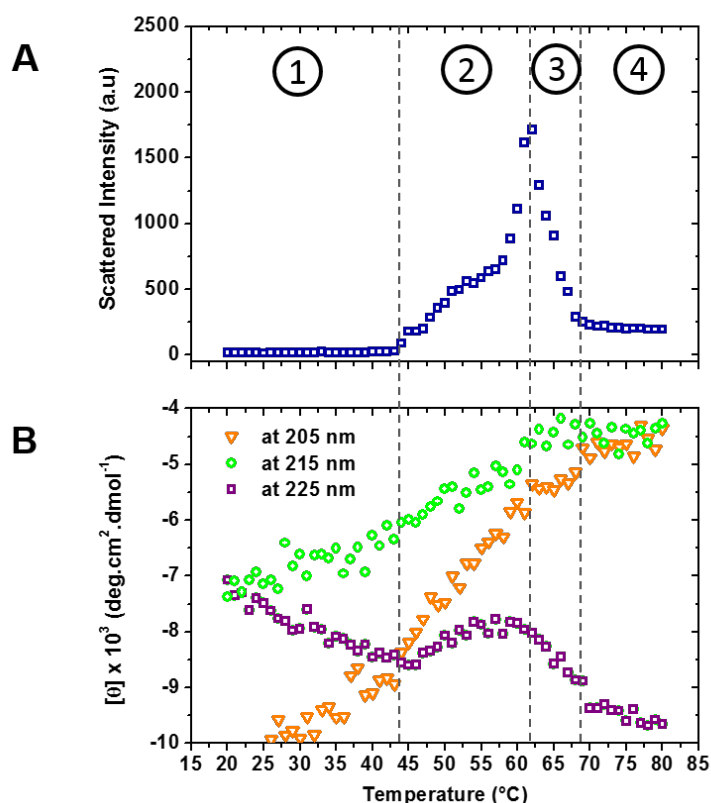


Figure 9. (A) Scattered light intensity (obtained by DLS at 90°) and (B) CD signals at 205 nm, 215 nm and 225 nm as a function of the temperature, obtained for a solution of PGlu₂₃-*b*-ELP at 14 μM in PBS.

As previously described, the scattered intensity showed a four-phase self-assembly behavior (Figure 9, panel A). Interestingly, the evolution of CD signals corresponding to the random coil conformation at 205 nm, to the type II β-turns at 215 nm and to the signal at 225 nm also revealed a different four-phase behavior. The first regime, corresponding to free diblock copolypeptide chains in solution, showed a gradual decrease of the proportion of random coil conformation to the benefit of a progressive formation of type II β-turns (signal at 215 nm) as

well as other ordered secondary structures (signal at 225 nm) upon temperature increase. The second regime, from the T_t (43 °C), corresponding to the aggregation phase, was coupled with a slightly faster decrease of the proportion of random coil conformation, gradual formation of type II β -turns, and a significant decrease of the signal of other secondary structures. The third regime started at the CMT at 62 °C with the drastic decrease in scattered light intensity corresponding to the formation of micelles. This step was also characterized by a slowdown of the decrease of the proportion of random coils, the stabilization of the proportion of type II β -turns and a rapid recovery of the formation of other secondary structures. Finally, the fourth regime, the stabilization of micellar structure, revealed the stabilization of the proportion of unordered structure and type II β -turns and a slight increase in the proportion of other secondary structures.

These observations are compatible to the hypothesis of Yingling and co-workers⁸⁸ arguing that increasing the temperature may first decrease the stability of intramolecular hydrogen bond, destabilizing the secondary structures, while higher temperatures can lead the recovery of secondary structures, likely due to the dehydration leading to a decrease of H-bonding with water and consequently an increase of intramolecular hydrogen bonding. This hypothesis is entirely plausible regarding the self-assembly of PGlu-*b*-ELP diblock copolypeptides since SANS measurements revealed a dehydration phenomenon within the micelles.

Conclusion

In this work, a thermoresponsive elastin-like polypeptide (ELP) was used as macroinitiator for the controlled ROP of γ -benzyl-*L*-glutamate *N*-carboxyanhydride (γ -BLG NCA) to access, after acid deprotection of BLG units, to well defined poly(*L*-glutamic acid)-*b*-ELP (PGlu-*b*-ELP)

hybrid diblock copolypeptides with different PGlu block lengths. PGlu₂₃-*b*-ELP, PGlu₄₅-*b*-ELP and PGlu₆₁-*b*-ELP were therefore efficiently synthesized to investigate their thermoresponsiveness using a combination of turbidimetry, mono- and multi-angle variable-temperature DLS and SLS, SANS, ¹H NMR and CD. Altogether these methods revealed the unexpected salt-dependent behavior of this series of diblock copolypeptides regarding their temperature-triggered self-assembly.

In ultrapure water, the diblock copolypeptides present a sharp two-phase solubility transition behavior from free chains to macroscopic aggregates. The transition temperatures (T_t) increased with the PGlu block length as a consequence of increased hydrophilicity of the diblock copolypeptide. This also led to a significant increase of the concentration dependence as over the T_t compare to native ELP. The design of PGlu-*b*-ELP diblock copolypeptides therefore allowed an easy tuning of the thermoresponsive behavior of the ELP using a convenient polymerization procedure.

Interestingly, the same diblock copolypeptides in phosphate-buffered saline (PBS) showed a completely different four-regime thermoresponsive behavior. Below the T_t , diblock copolypeptides were soluble and formed macroscopic aggregates above the T_t , which spontaneously evolved into well-defined nanoparticles at the CMT and finally reached an equilibrium. Small-angle neutron scattering measurements was used for a better understanding of the nanoparticles formation and evidenced a densification and dehydration phase, increasing the temperature above the CMT. The phenomena compensate each other, allowing the radii of the core to remain constant upon further temperature increase.

Figure 10 summarizes the proposed self-assembly mechanisms occurring in water and in PBS.

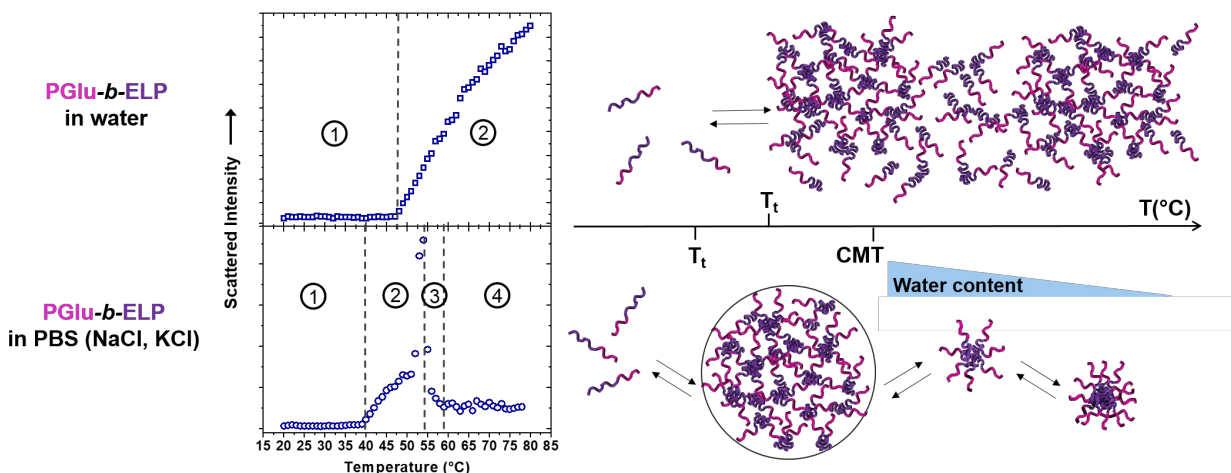


Figure 10. Schematic representation of the proposed self-assembly mechanisms of PGlu-*b*-ELP copolymers in water and in PBS.

At the molecular level, ^1H NMR and circular dichroism of native ELP revealed a strong folding process involving β -turns formation, occurring progressively in water and sharply in PBS. On the contrary, the NMR and CD studies of PGlu₂₃-*b*-ELP demonstrated the propensity of PGlu block to decrease the capacity of ELP block to form ordered structures in water. Interestingly, results obtained showed that this same diblock copolyptide, underwent a folding process in four steps in PBS. Above the T_t , during the aggregation step, proportion of secondary structures decreased, leading to less cohesive aggregates able to reorganize into nanoparticles, and increased again after reaching the CMT.

To summarize, our observations have suggested that the temperature-responsive self-assembly behavior of diblock copolyptides in PBS occurred *via* a mechanism involving both conformational changes due to a dehydration process and densification of micelle-like structure thanks to the presence of salt insuring both micellar core compaction and screening effect

between negatively charged Glu units in the shell. These findings demonstrated the utmost effect of the aqueous environment on the thermoresponsive properties of such hybrid synthetic recombinant diblock copolypeptides. This also highlights the importance of controlling both the macroscopic and the molecular interactions when designing responsive polymer systems, particularly based on such thermoresponsive ELPs.

ASSOCIATED CONTENT

Supporting Information. Molecular characteristics of diblock copolypeptides, additional spectra and figures, and description of the mixed model “polydisperse Sphere + Debye” for SANS are available free of charge via the Internet at <http://pubs.acs.org>.

AUTHOR INFORMATION

*Corresponding author: Sébastien Lecommandoux, Université de Bordeaux/Bordeaux INP, ENSCBP, 16 avenue Pey-Berland, 33607 Pessac Cedex, France. (E-mail: lecommandoux@enscbp.fr)

Conflicts of interest

There are no conflicts to declare.

ACKNOWLEDGMENTS

The authors thank Amélie Vax and Sophie Larnaudie from the Laboratoire de Chimie des Polymères Organiques for the SEC analyzes and general discussions respectively, Laëtitiya Minder from the Institut Européen de Chimie et Biologie for her assistance with the circular dichroism analyzes, Guillaume Goudounet for the ELP production and Bertand Garbay for

discussions.

This work benefited from the use of the SasView application, originally developed under NSF award DMR-0520547.

References

1. Stuart, M. A. C.; Huck, W. T.; Genzer, J.; Müller, M.; Ober, C.; Stamm, M.; Sukhorukov, G. B.; Szleifer, I.; Tsukruk, V. V.; Urban, M., Emerging applications of stimuli-responsive polymer materials. *Nat. Mater.* **2010**, *9* (2), 101.
2. Ward, M. A.; Georgiou, T. K., Thermoresponsive polymers for biomedical applications. *Polymers* **2011**, *3* (3), 1215-1242.
3. Weber, C.; Hoogenboom, R.; Schubert, U. S., Temperature responsive bio-compatible polymers based on poly (ethylene oxide) and poly (2-oxazoline) s. *Prog. Polym. Sci.* **2012**, *37* (5), 686-714.
4. Seuring, J.; Agarwal, S., Polymers with upper critical solution temperature in aqueous solution. *Macromol. Rapid Commun.* **2012**, *33* (22), 1898-1920.
5. Agut, W.; Brûlet, A.; Taton, D.; Lecommandoux, S., Thermoresponsive micelles from jeffamine-b-poly (L-glutamic acid) double hydrophilic block copolymers. *Langmuir* **2007**, *23* (23), 11526-11533.
6. Akimoto, J.; Nakayama, M.; Sakai, K.; Okano, T., Temperature-induced intracellular uptake of thermoresponsive polymeric micelles. *Biomacromolecules* **2009**, *10* (6), 1331-1336.
7. Akimoto, J.; Nakayama, M.; Okano, T., Temperature-responsive polymeric micelles for optimizing drug targeting to solid tumors. *J. Controlled Release* **2014**, *193*, 2-8.
8. Lee, Y.; Chung, H. J.; Yeo, S.; Ahn, C.-H.; Lee, H.; Messersmith, P. B.; Park, T. G., Thermo-sensitive, injectable, and tissue adhesive sol–gel transition hyaluronic acid/pluronic composite hydrogels prepared from bio-inspired catechol-thiol reaction. *Soft Matter* **2010**, *6* (5), 977-983.
9. Jeong, B.; Kim, S. W.; Bae, Y. H., Thermosensitive sol–gel reversible hydrogels. *Adv. Drug Delivery Rev.* **2012**, *64*, 154-162.
10. Vaupel, P.; Kallinowski, F.; Okunieff, P., Blood flow, oxygen and nutrient supply, and metabolic microenvironment of human tumors: a review. *Cancer Res.* **1989**, *49* (23), 6449-6465.
11. Abulateefeh, S. R.; Spain, S. G.; Aylott, J. W.; Chan, W. C.; Garnett, M. C.; Alexander, C., Thermoresponsive polymer colloids for drug delivery and cancer therapy. *Macromol. Biosci.* **2011**, *11* (12), 1722-1734.
12. Aqil, A.; Vasseur, S.; Duguet, E.; Passirani, C.; Benoît, J.-P.; Jérôme, R.; Jérôme, C., Magnetic nanoparticles coated by temperature responsive copolymers for hyperthermia. *J. Mater. Chem.* **2008**, *18* (28), 3352-3360.
13. Louguet, S.; Rousseau, B.; Epherre, R.; Guidolin, N.; Goglio, G.; Mornet, S.; Duguet, E.; Lecommandoux, S.; Schatz, C., Thermoresponsive polymer brush-functionalized magnetic manganite nanoparticles for remotely triggered drug release. *Polym. Chem.* **2012**, *3* (6), 1408-1417.
14. Hemery, G.; Garanger, E.; Lecommandoux, S.; Wong, A. D.; Gillies, E. R.; Pedrono, B.; Bayle, T.; Jacob, D.; Sandre, O., Thermosensitive polymer-grafted iron oxide nanoparticles studied by in situ dynamic light backscattering under magnetic hyperthermia. *J. Phys. D: Appl. Phys.* **2015**, *48* (49), 494001.

15. Hervault, A.; Dunn, A. E.; Lim, M.; Boyer, C.; Mott, D.; Maenosono, S.; Thanh, N. T., Doxorubicin loaded dual pH-and thermo-responsive magnetic nanocarrier for combined magnetic hyperthermia and targeted controlled drug delivery applications. *Nanoscale* **2016**, *8* (24), 12152-12161.
16. Halperin, A.; Kröger, M.; Winnik, F. M., Poly (N-isopropylacrylamide) Phase Diagrams: Fifty Years of Research. *Angew. Chem., Int. Ed.* **2015**, *54* (51), 15342-15367.
17. Schild, H. G., Poly (N-isopropylacrylamide): experiment, theory and application. *Prog. Polym. Sci.* **1992**, *17* (2), 163-249.
18. Cortez-Lemus, N. A.; Licea-Claverie, A., Poly (N-vinylcaprolactam), a comprehensive review on a thermoresponsive polymer becoming popular. *Prog. Polym. Sci.* **2016**, *53*, 1-51.
19. Liu, J.; Debuigne, A.; Detrembleur, C.; Jérôme, C., Poly (N-vinylcaprolactam): A Thermoresponsive Macromolecule with Promising Future in Biomedical Field. *Adv. Healthcare Mater.* **2014**, *3* (12), 1941-1968.
20. Ramos, J.; Imaz, A.; Forcada, J., Temperature-sensitive nanogels: poly (N-vinylcaprolactam) versus poly (N-isopropylacrylamide). *Polym. Chem.* **2012**, *3* (4), 852-856.
21. Hoogenboom, R.; Schlaad, H., Thermoresponsive poly (2-oxazoline) s, polypeptoids, and polypeptides. *Polym. Chem.* **2017**, *8* (1), 24-40.
22. Le Fer, G.; Amiel, C.; Volet, G., Copolymers based on azidopentyl-2-oxazoline: synthesis, characterization and LCST behavior. *Eur. Polym. J.* **2015**, *71*, 523-533.
23. Legros, C.; De Pauw-Gillet, M.-C.; Tam, K. C.; Taton, D.; Lecommandoux, S., Crystallisation-driven self-assembly of poly (2-isopropyl-2-oxazoline)-block-poly (2-methyl-2-oxazoline) above the LCST. *Soft Matter* **2015**, *11* (17), 3354-3359.
24. Le Fer, G.; Babinot, J.; Versace, D. L.; Langlois, V.; Renard, E., An Efficient Thiol-Ene Chemistry for the Preparation of Amphiphilic PHA-Based Graft Copolymers. *Macromol. Rapid Commun.* **2012**, *33* (23), 2041-2045.
25. Niu, G.; Zhang, H.; Song, L.; Cui, X.; Cao, H.; Zheng, Y.; Zhu, S.; Yang, Z.; Yang, H., Thiol/acrylate-modified PEO-PPO-PEO triblocks used as reactive and thermosensitive copolymers. *Biomacromolecules* **2008**, *9* (10), 2621-2628.
26. Lutz, J.-F.; Hoth, A., Preparation of ideal PEG analogues with a tunable thermosensitivity by controlled radical copolymerization of 2-(2-methoxyethoxy) ethyl methacrylate and oligo (ethylene glycol) methacrylate. *Macromolecules* **2006**, *39* (2), 893-896.
27. Yamamoto, S.-i.; Pietrasik, J.; Matyjaszewski, K., ATRP synthesis of thermally responsive molecular brushes from oligo (ethylene oxide) methacrylates. *Macromolecules* **2007**, *40* (26), 9348-9353.
28. Lutz, J. F., Polymerization of oligo (ethylene glycol)(meth) acrylates: Toward new generations of smart biocompatible materials. *J. Polym. Sci., Part A: Polym. Chem.* **2008**, *46* (11), 3459-3470.
29. Roth, P. J.; Jochum, F. D.; Forst, F. R.; Zentel, R.; Theato, P., Influence of End Groups on the Stimulus-Responsive Behavior of Poly [oligo (ethylene glycol) methacrylate] in Water. *Macromolecules* **2010**, *43* (10), 4638-4645.

30. Miasnikova, A.; Laschewsky, A., Influencing the phase transition temperature of poly (methoxy diethylene glycol acrylate) by molar mass, end groups, and polymer architecture. *J. Polym. Sci., Part A: Polym. Chem.* **2012**, *50* (16), 3313-3323.
31. Chopko, C. M.; Lowden, E. L.; Engler, A. C.; Griffith, L. G.; Hammond, P. T., Dual responsiveness of a tunable thermosensitive polypeptide. *ACS Macro Lett.* **2012**, *1* (6), 727-731.
32. Wu, Y.; Deng, Y.; Yuan, Q.; Ling, Y.; Tang, H., Thermoresponsive poly (γ -propyl-l-glutamate)-graft-(oligo ethylene glycol) s: Synthesis, characterization, and properties. *J. Appl. Polym. Sci.* **2014**, *131* (21), 41022-41028.
33. Gharakhanian, E. G.; Deming, T. J., Role of side-chain molecular features in tuning lower critical solution temperatures (LCSTs) of oligoethylene glycol modified polypeptides. *J. Phys. Chem. B* **2016**, *120* (26), 6096-6101.
34. Yan, J.; Liu, K.; Li, W.; Shi, H.; Zhang, A., Thermoresponsive Dendronized Polypeptides Showing Switchable Recognition to Catechols. *Macromolecules* **2016**, *49* (2), 510-517.
35. Fu, X.; Shen, Y.; Fu, W.; Li, Z., Thermoresponsive Oligo (ethylene glycol) Functionalized Poly-l-cysteine. *Macromolecules* **2013**, *46* (10), 3753-3760.
36. Ruff, K. M.; Roberts, S.; Chilkoti, A.; Pappu, R. V., Advances in Understanding Stimulus Responsive Phase Behavior of Intrinsically Disordered Protein Polymers. *J. Mol. Biol.* **2018**, 4619-4635.
37. MacEwan, S. R.; Chilkoti, A., Applications of elastin-like polypeptides in drug delivery. *J. Controlled Release* **2014**, *190*, 314-330.
38. Glassman, M. J.; Avery, R. K.; Khademhosseini, A.; Olsen, B. D., Toughening of thermoresponsive arrested networks of elastin-like polypeptides to engineer cytocompatible tissue scaffolds. *Biomacromolecules* **2016**, *17* (2), 415-426.
39. Meyer, D. E.; Chilkoti, A., Quantification of the effects of chain length and concentration on the thermal behavior of elastin-like polypeptides. *Biomacromolecules* **2004**, *5* (3), 846-851.
40. Meyer, D. E.; Chilkoti, A., Genetically encoded synthesis of protein-based polymers with precisely specified molecular weight and sequence by recursive directional ligation: examples from the elastin-like polypeptide system. *Biomacromolecules* **2002**, *3* (2), 357-367.
41. Urry, D. W.; Trapane, T.; Prasad, K., Phase-structure transitions of the elastin polypeptide–water system within the framework of composition–temperature studies. *Biopolymers* **1985**, *24* (12), 2345-2356.
42. Urry, D. W., Physical chemistry of biological free energy transduction as demonstrated by elastic protein-based polymers. *J. Phys. Chem. B* **1997**, *101* (51), 11007-11028.
43. MacEwan, S. R.; Weitzhandler, I.; Hoffmann, I.; Genzer, J.; Gradzielski, M.; Chilkoti, A., Phase behavior and self-assembly of perfectly sequence-defined and monodisperse multiblock copolypeptides. *Biomacromolecules* **2017**, *18* (2), 599-609.
44. Simon, J. R.; Carroll, N. J.; Rubinstein, M.; Chilkoti, A.; López, G. P., Programming molecular self-assembly of intrinsically disordered proteins containing sequences of low complexity. *Nat. Chem.* **2017**, *9* (6), 509.

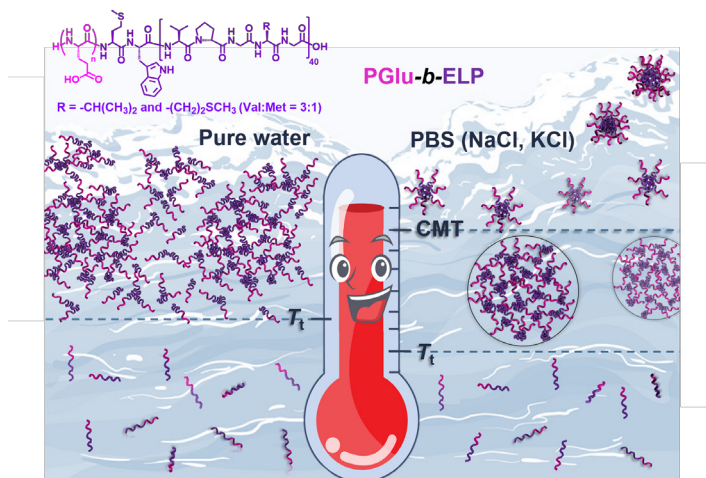
45. Li, N. K.; Roberts, S.; Quiroz, F. G.; Chilkoti, A.; Yingling, Y. G., Sequence directionality dramatically affects LCST behavior of elastin-like polypeptides. *Biomacromolecules* **2018**, 2496–2505.
46. Kramer, J. R.; Petitdemange, R.; Bataille, L.; Bathany, K.; Wirotius, A.-L.; Garbay, B.; Deming, T. J.; Garanger, E.; Lecommandoux, S., Quantitative Side-Chain Modifications of Methionine-Containing Elastin-Like Polypeptides as a Versatile Tool to Tune Their Properties. *ACS Macro Lett.* **2015**, 4 (11), 1283-1286.
47. Petitdemange, R.; Garanger, E.; Bataille, L.; Bathany, K.; Garbay, B.; Deming, T. J.; Lecommandoux, S., Tuning Thermo-responsive Properties of Cationic Elastin-like Polypeptides by Varying Counterions and Side-Chains. *Bioconjugate Chem.* **2017**, 28 (5), 1403-1412.
48. Petitdemange, R.; Garanger, E.; Bataille, L.; Dieryck, W.; Bathany, K.; Garbay, B.; Deming, T. J.; Lecommandoux, S., Selective tuning of elastin-like polypeptide properties via methionine oxidation. *Biomacromolecules* **2017**, 18 (2), 544-550.
49. McDaniel, J. R.; Callahan, D. J.; Chilkoti, A., Drug delivery to solid tumors by elastin-like polypeptides. *Adv. Drug Delivery Rev.* **2010**, 62 (15), 1456-1467.
50. Dreher, M. R.; Raucher, D.; Balu, N.; Colvin, O. M.; Ludeman, S. M.; Chilkoti, A., Evaluation of an elastin-like polypeptide–doxorubicin conjugate for cancer therapy. *J. Controlled Release* **2003**, 91 (1), 31-43.
51. MacKay, J. A.; Chen, M.; McDaniel, J. R.; Liu, W.; Simnick, A. J.; Chilkoti, A., Self-assembling chimeric polypeptide-doxorubicin conjugate nanoparticles that abolish tumors after a single injection. *Nat. Mater.* **2009**, 8 (12), 993.
52. Tao, X.; Deng, Y.; Shen, Z.; Ling, J., Controlled polymerization of N-substituted glycine N-thiocarboxyanhydrides initiated by rare earth borohydrides toward hydrophilic and hydrophobic polypeptoids. *Macromolecules* **2014**, 47 (18), 6173-6180.
53. Urry, D. W., Entropic elastic processes in protein mechanisms. I. Elastic structure due to an inverse temperature transition and elasticity due to internal chain dynamics. *J. Protein Chem.* **1988**, 7 (1), 1-34.
54. Schmaljohann, D., Thermo- and pH-responsive polymers in drug delivery. *Adv. Drug Delivery Rev.* **2006**, 58 (15), 1655-1670.
55. Luan, C. H.; Parker, T. M.; Prasad, K. U.; Urry, D. W., Differential scanning calorimetry studies of NaCl effect on the inverse temperature transition of some elastin-based polytetra-, poly-penta-, and polynona-peptides. *Biopolymers* **1991**, 31 (5), 465-475.
56. Urry, D. W., Physical chemistry of biological free energy transduction as demonstrated by elastic protein-based polymers. *Journal of Physical Chemistry B* **1997**, 101, 11007-11028.
57. Reguera, J.; Urry, D. W.; Parker, T. M.; McPherson, D. T.; Rodríguez-Cabello, J. C., Effect of NaCl on the exothermic and endothermic components of the inverse temperature transition of a model elastin-like polymer. *Biomacromolecules* **2007**, 8 (2), 354-358.
58. Sallach, R. E.; Wei, M.; Biswas, N.; Conticello, V. P.; Lecommandoux, S.; Dluhy, R. A.; Chaikof, E. L., Micelle density regulated by a reversible switch of protein secondary structure. *J. Am. Chem. Soc.* **2006**, 128 (36), 12014-12019.

59. Dreher, M. R.; Simnick, A. J.; Fischer, K.; Smith, R. J.; Patel, A.; Schmidt, M.; Chilkoti, A., Temperature triggered self-assembly of polypeptides into multivalent spherical micelles. *J. Am. Chem. Soc.* **2008**, *130* (2), 687-694.
60. Kim, W.; Thévenot, J.; Ibarboure, E.; Lecommandoux, S.; Chaikof, E. L., Self-assembly of thermally responsive amphiphilic diblock copolypeptides into spherical micellar nanoparticles. *Angew. Chem.* **2010**, *122* (25), 4353-4356.
61. Garanger, E.; MacEwan, S. R.; Sandre, O.; Brûlet, A.; Bataille, L.; Chilkoti, A.; Lecommandoux, S. b., Structural evolution of a stimulus-responsive diblock polypeptide micelle by temperature tunable compaction of its core. *Macromolecules* **2015**, *48* (18), 6617-6627.
62. Hassouneh, W.; Zhulina, E. B.; Chilkoti, A.; Rubinstein, M., Elastin-like polypeptide diblock copolymers self-assemble into weak micelles. *Macromolecules* **2015**, *48* (12), 4183-4195.
63. van Eldijk, M. B.; Smits, F. C.; Vermue, N.; Debets, M. F.; Schoffelen, S.; van Hest, J. C., Synthesis and self-assembly of well-defined elastin-like polypeptide-poly (ethylene glycol) conjugates. *Biomacromolecules* **2014**, *15* (7), 2751-2759.
64. Bonduelle, C.; Makni, F.; Severac, L.; Piedra-Arroni, E.; Serpentine, C.-L.; Lecommandoux, S.; Pratviel, G., Smart metallopoly (L-glutamic acid) polymers: reversible helix-to-coil transition at neutral pH. *RSC Adv.* **2016**, *6* (88), 84694-84697.
65. Hadjichristidis, N.; Iatrou, H.; Pitsikalis, M.; Sakellariou, G., Synthesis of well-defined polypeptide-based materials via the ring-opening polymerization of α -amino acid N-carboxyanhydrides. *Chem. Rev.* **2009**, *109* (11), 5528-5578.
66. Cheng, J.; Deming, T. J., Synthesis of polypeptides by ring-opening polymerization of α -amino acid N-carboxyanhydrides. In *Peptide-based materials*, Springer: 2011; pp 1-26.
67. Huang, J.; Heise, A., Stimuli responsive synthetic polypeptides derived from N-carboxyanhydride (NCA) polymerisation. *Chem. Soc. Rev.* **2013**, *42* (17), 7373-7390.
68. Le Fer, G.; Portes, D.; Goudounet, G.; Guigner, J.-M.; Garanger, E.; Lecommandoux, S., Design and self-assembly of PBLG-b-ELP hybrid diblock copolymers based on synthetic and elastin-like polypeptides. *Org. Biomol. Chem.* **2017**, *15* (47), 10095-10104.
69. Ribeiro, A.; Arias, F. J.; Reguera, J.; Alonso, M.; Rodríguez-Cabello, J. C., Influence of the amino-acid sequence on the inverse temperature transition of elastin-like polymers. *Biophys. J.* **2009**, *97* (1), 312-320.
70. Zhang, Q.; Wilson, P.; Anastasaki, A.; McHale, R.; Haddleton, D. M., Synthesis and aggregation of double hydrophilic diblock glycopolymers via aqueous SET-LRP. *ACS Macro Lett.* **2014**, *3* (5), 491-495.
71. Agut, W.; Brûlet, A.; Schatz, C.; Taton, D.; Lecommandoux, S., pH and temperature responsive polymeric micelles and polymersomes by self-assembly of poly [2-(dimethylamino) ethyl methacrylate]-b-poly (glutamic acid) double hydrophilic block copolymers. *Langmuir* **2010**, *26* (13), 10546-10554.
72. Weitzhandler, I.; Dzuricky, M.; Hoffmann, I.; Garcia Quiroz, F.; Gradzielski, M.; Chilkoti, A., Micellar Self-Assembly of Recombinant Resilin/Elastin-Like Block Copolypeptides. *Biomacromolecules* **2017**, *18* (8), 2419-2426.

73. Urry, D. W.; Gowda, D.; Parker, T. M.; Luan, C. H.; Reid, M. C.; Harris, C. M.; Pattanaik, A.; Harris, R. D., Hydrophobicity scale for proteins based on inverse temperature transitions. *Biopolymers* **1992**, *32* (9), 1243-1250.
74. Cho, Y.; Sagle, L. B.; Iimura, S.; Zhang, Y.; Kherb, J.; Chilkoti, A.; Scholtz, J. M.; Cremer, P. S., Hydrogen bonding of β -turn structure is stabilized in D₂O. *J. Am. Chem. Soc.* **2009**, *131* (42), 15188-15193.
75. Sun, S. T.; Nishio, I.; Swislow, G.; Tanaka, T., The coil-globule transition: radius of gyration of polystyrene in cyclohexane. *J. Chem. Phys.* **1980**, *73* (12), 5971-5975.
76. Higashi, N.; Sekine, D.; Koga, T., Temperature induced self-assembly of amino acid-derived vinyl block copolymers via dual phase transitions. *J. Colloid Interface Sci.* **2017**, *500*, 341-348.
77. Trinh, L. T.; Lambermont-Thijs, H. M.; Schubert, U. S.; Hoogenboom, R.; Kjøniksen, A.-L., Thermoresponsive poly (2-oxazoline) block copolymers exhibiting two cloud points: complex multistep assembly behavior. *Macromolecules* **2012**, *45* (10), 4337-4345.
78. Guiner, A.; Fournet, G.; Walker, C., Small angle scattering of X-rays. *J. Wiley & Sons, New York* **1955**.
79. Andersson, K.; Hovmöller, S., The average atomic volume and density of proteins. *Zeitschrift Fur Kristallographie* **1998**, *213* (7), 369-373.
80. Janib, S. M.; Pastuszka, M.; Aluri, S.; Folchman-Wagner, Z.; Hsueh, P.; Shi, P.; Lin, Y.; Cui, H.; Mackay, J., A quantitative recipe for engineering protein polymer nanoparticles. *Polym. Chem.* **2014**, *5* (5), 1614-1625.
81. Lee, T.; Cooper, A.; Apkarian, R. P.; Conticello, V., Thermo-reversible self-assembly of nanoparticles derived from elastin-mimetic polypeptides. *Adv. Mater.* **2000**, *12* (15), 1105-1110.
82. Borisov, O.; Zhulina, E., Effect of salt on self-assembly in charged block copolymer micelles. *Macromolecules* **2002**, *35* (11), 4472-4480.
83. Dan, N.; Tirrell, M., Self-assembly of block copolymers with a strongly charged and a hydrophobic block in a selective, polar solvent. Micelles and adsorbed layers. *Macromolecules* **1993**, *26* (16), 4310-4315.
84. Gottlieb, H. E.; Kotlyar, V.; Nudelman, A., NMR chemical shifts of common laboratory solvents as trace impurities. *J. Org. Chem.* **1997**, *62* (21), 7512-7515.
85. Zeng, F.; Tong, Z.; Feng, H., NMR investigation of phase separation in poly (N-isopropyl acrylamide)/water solutions. *Polymer* **1997**, *38* (22), 5539-5544.
86. Spěvák, J., NMR investigations of phase transition in aqueous polymer solutions and gels. *Curr. Opin. Colloid Interface Sci.* **2009**, *14* (3), 184-191.
87. Spěvák, J.; Dybal, J.; Starovoytova, L.; Zhigunov, A.; Sedláková, Z., Temperature-induced phase separation and hydration in poly (N-vinylcaprolactam) aqueous solutions: a study by NMR and IR spectroscopy, SAXS, and quantum-chemical calculations. *Soft Matter* **2012**, *8* (22), 6110-6119.

88. Li, N. K.; Quiroz, F. G.; Hall, C. K.; Chilkoti, A.; Yingling, Y. G., Molecular description of the LCST behavior of an elastin-like polypeptide. *Biomacromolecules* **2014**, *15* (10), 3522-3530.
89. Chécot, F.; Brûlet, A.; Oberdisse, J.; Gnanou, Y.; Mondain-Monval, O.; Lecommandoux, S., Structure of polypeptide-based diblock copolymers in solution: Stimuli-responsive vesicles and micelles. *Langmuir* **2005**, *21* (10), 4308-4315.
90. Roberts, S.; Dzuricky, M.; Chilkoti, A., Elastin-like polypeptides as models of intrinsically disordered proteins. *FEBS Lett.* **2015**, *589* (19), 2477-2486.
91. Reiersen, H.; Clarke, A. R.; Rees, A. R., Short elastin-like peptides exhibit the same temperature-induced structural transitions as elastin polymers: implications for protein engineering¹. *J. Mol. Biol.* **1998**, *283* (1), 255-264.
92. Nuhn, H.; Klok, H.-A., Secondary structure formation and LCST behavior of short elastin-like peptides. *Biomacromolecules* **2008**, *9* (10), 2755-2763.
93. Vrhovski, B.; Jensen, S.; Weiss, A. S., Coacervation characteristics of recombinant human tropoelastin. *Eur. J. Biochem.* **1997**, *250* (1), 92-98.
94. Li, B.; Daggett, V., The molecular basis of the temperature-and pH-induced conformational transitions in elastin-based peptides. *Biopolymers* **2003**, *68* (1), 121-129.
95. Wu, I. L.; Patterson, M. A.; Carpenter Desai, H. E.; Mehl, R. A.; Giorgi, G.; Conticello, V. P., Multiple Site-Selective Insertions of Noncanonical Amino Acids into Sequence-Repetitive Polypeptides. *ChemBioChem* **2013**, *14* (8), 968-978.
96. Urry, D. W., Protein elasticity based on conformations of sequential polypeptides: the biological elastic fiber. *J. Protein Chem.* **1984**, *3* (5-6), 403-436.
97. Rodríguez-Cabello, J. C.; Alonso, M.; Pérez, T.; Herguedas, M. M., Differential scanning calorimetry study of the hydrophobic hydration of the elastin-based polypentapeptide, poly (VPGVG), from deficiency to excess of water. *Biopolymers* **2000**, *54* (4), 282-288.
98. Yao, X.; Hong, M., Structure distribution in an elastin-mimetic peptide (VPGVG) ³ investigated by solid-state NMR. *J. Am. Chem. Soc.* **2004**, *126* (13), 4199-4210.
99. Groß, P. C.; Possart, W.; Zeppezauer, M., An alternative structure model for the polypentapeptide in elastin. *Zeitschrift für Naturforschung C* **2003**, *58* (11-12), 873-878.
100. Bochicchio, B.; Tamburro, A. M., Polyproline II structure in proteins: identification by chiroptical spectroscopies, stability, and functions. *Chirality* **2002**, *14* (10), 782-792.

TABLE OF CONTENT



SUPPORTING INFORMATIONS

Self-assembly of stimuli-responsive biohybrid synthetic-*b*-recombinant block copolypeptides

Gaëlle Le Fer^{§†}, Anne-Laure Wirotius^{§†}, Annie Brûlet[‡], Elisabeth Garanger^{§†}, Sébastien Lecommandoux^{*§†}

§ Université de Bordeaux, Bordeaux INP, ENSCBP, 16 avenue Pey-Berland, 33607 Pessac Cedex, France, † CNRS, Laboratoire de Chimie des Polymères Organiques (UMR5629), Pessac, France, ‡ Laboratoire Léon Brillouin, UMR 12 CEA–CNRS, CEA Saclay, 91191 Gif-sur-Yvette Cedex, France.

*Correspondence to: Sébastien Lecommandoux (E-mail: lecommandoux@enscbp.fr)

Contents

Figure S1. ¹ H NMR spectrum of ELP in CDCl ₃ containing 15 % trifluoroacetic acid (TFA). 3	3
Figure S2. ¹ H NMR spectra of (A) poly(γ-benzyl- <i>L</i> -glutamate) ₂₃ - <i>block</i> -ELP in CDCl ₃ (+ 15 % TFA) and (B) poly(<i>L</i> -glutamic acid) ₂₃ - <i>block</i> -ELP in DMSO- <i>d</i> ₆ (+ 15 % TFA). 4	4
Figure S3. Size exclusion chromatography profiles of ELP and copolypeptides PBLG- <i>b</i> -ELP (before deprotection). 5	5
Figure S4. Evolution of absorbance with temperature of solutions of PGlu ₂₃ - <i>b</i> -ELP, PGlu ₄₅ - <i>b</i> -ELP and PGlu ₆₁ - <i>b</i> -ELP diblock copolypeptides at 1 g.L ⁻¹ in pure water during heating (filled symbols) and cooling (empty symbols), for two successive cycles, to demonstrate reversible phase behavior. 5	5
Figure S5. Evolution of the scattered light intensity with temperature of a solution of PGlu ₂₃ - <i>b</i> -ELP in pure water at 1 g.L ⁻¹ (values obtained by DLS light scattering measurements at 90°). 6	6
Figure S6. Evolution of absorbance of solutions of PGlu ₂₃ - <i>b</i> -ELP diblock copolypeptide with temperature at 1.g.L ⁻¹ in H ₂ O and in D ₂ O (left) and in H ₂ O-PBS and D ₂ O-PBS (right). 6	6

Figure S7. Small-angle neutron scattering intensity as a function of q for PGlu ₂₃ - <i>b</i> -ELP solution at 1 mg.mL ⁻¹ in D ₂ O at 25°C (< T_t) and at 65°C (> T_t).	7
Figure S8. Evolution of absorbance of solutions of PGlu ₂₃ - <i>b</i> -ELP with temperature at 1.g.L ⁻¹ in a phosphate buffer (Na ₂ HPO ₄ 8 mM, KH ₂ PO ₄ 2 mM, pH = 7.2) and different concentrations of NaCl (from 0 to 137 mM).	7
Figure S9. (A, D) Scattered light intensity, (B, E) average hydrodynamic radius and (C, F) polydispersity index <i>versus</i> temperature of solutions of PGlu ₄₅ - <i>b</i> -ELP (left) and PGlu ₆₁ - <i>b</i> -ELP (right) diblock copolypeptide at 1 g.L ⁻¹ in PBS (values obtained by DLS measurements at 90°).	8
Figure S10. Evolution of absorbance with temperature of solutions of PGlu ₂₃ - <i>b</i> -ELP, PGlu ₄₅ - <i>b</i> -ELP and PGlu ₆₁ - <i>b</i> -ELP diblock copolypeptides at 1 g.L ⁻¹ in PBS during heating (filled symbols) and cooling (empty symbols) to demonstrate reversible phase behavior.	9
Figure S11. Small-angle neutron scattering of solutions of PGlu- <i>b</i> -ELP diblock copolypeptides prepared at 1 mg.mL ⁻¹ in D ₂ O-PBS. (A) Scattering intensity as a function of q for PGlu ₄₅ - <i>b</i> -ELP at various temperatures; the solid line are the fitting curves by a polydisperse Sphere Model. (B) Scattering intensity as a function of q for PGlu ₆₁ - <i>b</i> -ELP at various temperatures; the solid line are the fitting curves obtained by using a polydisperse sphere model (except for the data obtained at 45°C, the model used is a mixed model of the polydisperse Sphere and the Debye models).	11
Figure S12. Small-angle neutron scattering intensity as a function of q for PGlu ₂₃ - <i>b</i> -ELP solution at 1 mg.mL ⁻¹ in D ₂ O and in D ₂ O with 1 eq of NaOD / carboxylic acid group (pD = 9) at 65°C (> T_t).	12
Figure S13. (A) ¹ H NMR spectra of PGlu ₂₃ - <i>b</i> -ELP in D ₂ O (1 g.L ⁻¹) at various temperature. (B) Phase separation p-fraction from ¹ H NMR signals A, B, C, D and E plotted as a function of the temperature.	13
Figure S14. Temperature-dependence of the mean molar residue ellipticities at 205 nm, 215 nm and 225 nm of ELP in pure water (A) PGlu ₂₃ - <i>b</i> -ELP in pure water (B) and ELP in PBS (C) and PGlu ₂₃ - <i>b</i> -ELP in PBS (D) at 9 μM.	14

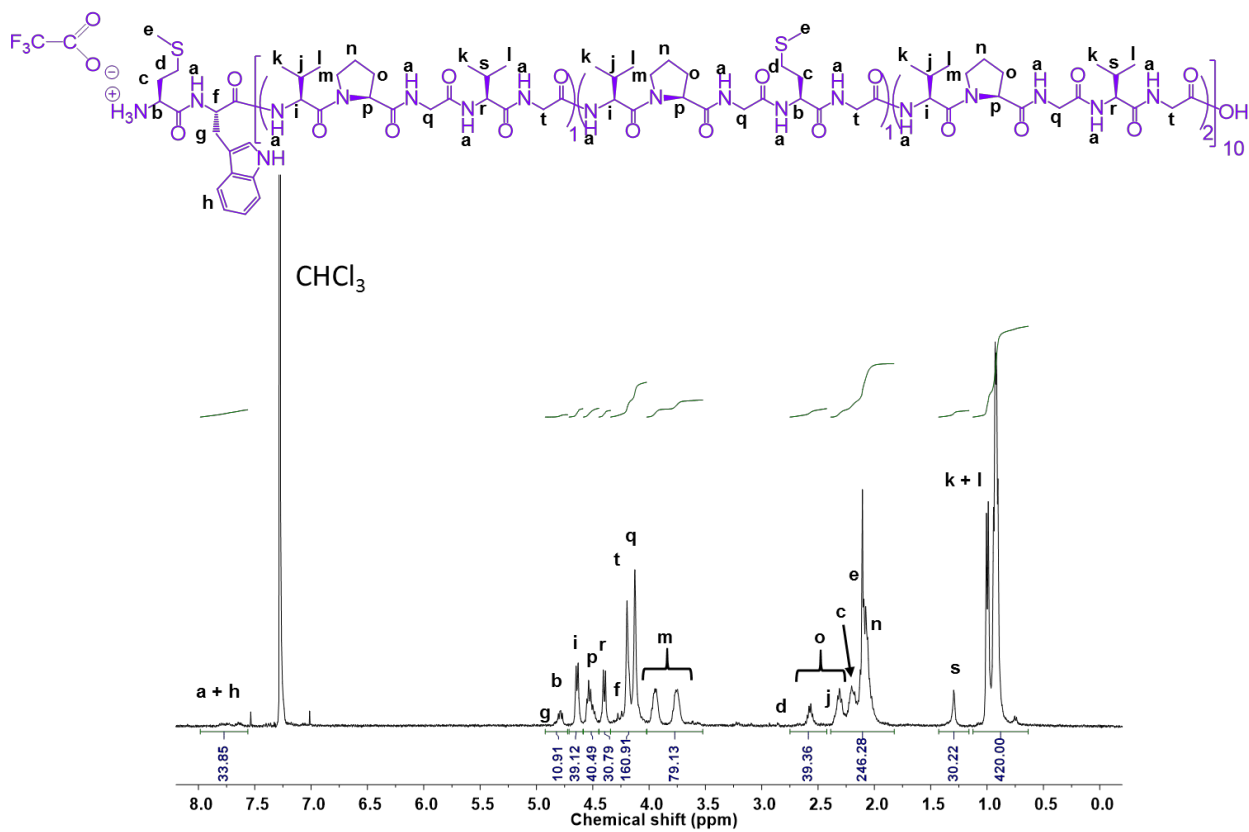


Figure S1. ^1H NMR spectrum of ELP in CDCl_3 containing 15 % trifluoroacetic acid (TFA).

The ^1H NMR in CDCl_3 (with 15% TFA) of the poly(γ -benzyl-*L*-glutamate)-*block*-ELP diblock copolypeptides allowed the calculation of the degrees of polymerization (DP) of the PBLG blocks by comparing the integral of the peak 2 at 5.10 ppm corresponding to the methylene group in α of the benzyl ring of the BLG units ($2\ ^1\text{H}$ per BLG unit) and the integral of the resonance peak (k+l) at 0.94 ppm from the ELP (*vide supra*, $420\ ^1\text{H}$) (Figure S2, panel A). The ^1H NMR in DMSO-d_6 (with 15% TFA) of the poly(*L*-glutamic acid)-*block*-ELP diblock copolypeptides confirmed the total deprotection of the carboxylic acid groups with the disappearance of the signal 2 at 5.10 ppm corresponding to the methylene group of the BLG units in α of the removed benzyl ring (Figure S2, panel B).

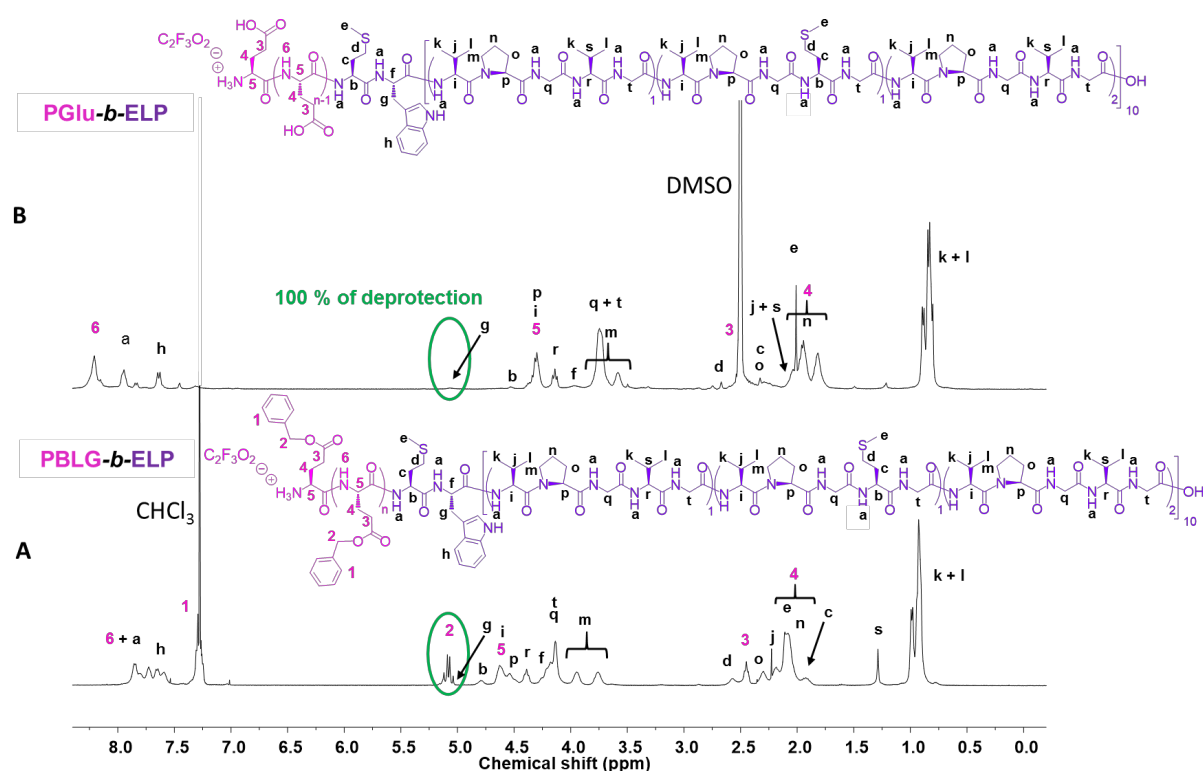


Figure S2. ^1H NMR spectra of (A) poly(γ -benzyl-*L*-glutamate)₂₃-*block*-ELP in CDCl_3 (+ 15 % TFA) and (B) poly(*L*-glutamic acid)₂₃-*block*-ELP in DMSO-d_6 (+ 15 % TFA).

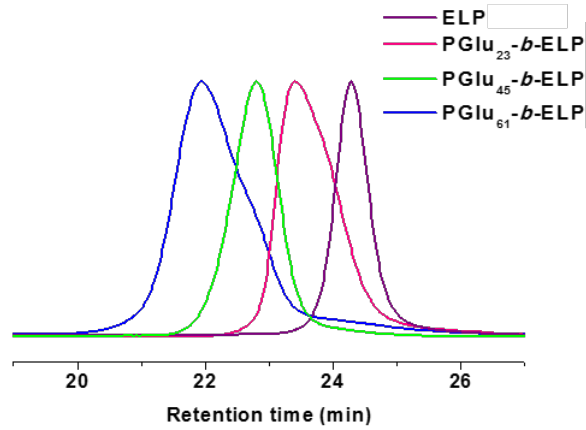


Figure S3. Size exclusion chromatography profiles of ELP and copolypeptides PBLG-*b*-ELP (before deprotection).

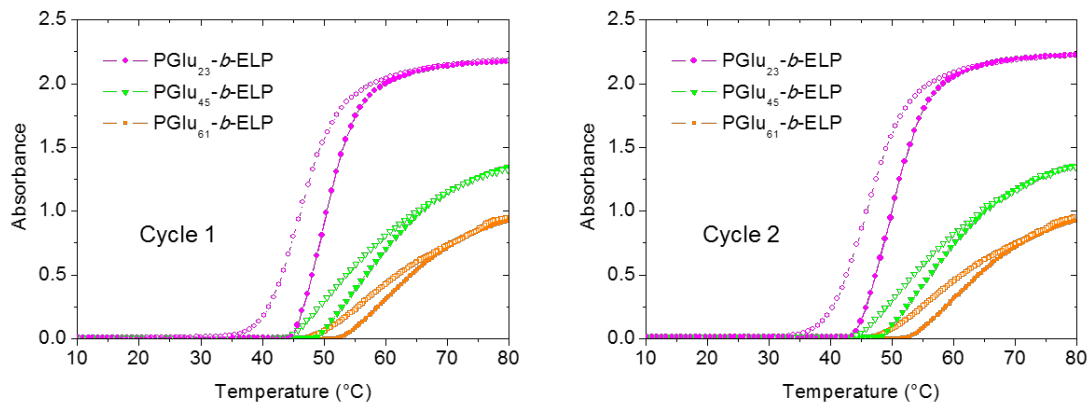


Figure S4. Evolution of absorbance with temperature of solutions of PGlu₂₃-*b*-ELP, PGlu₄₅-*b*-ELP and PGlu₆₁-*b*-ELP diblock copolypeptides at 1 g.L⁻¹ in pure water during heating (filled symbols) and cooling (empty symbols), for two successive cycles, to demonstrate reversible phase behavior.

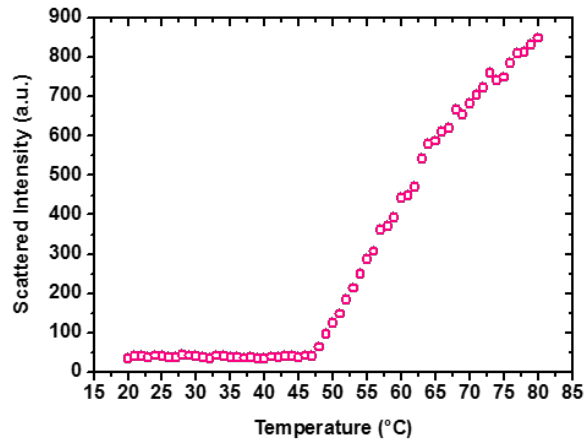


Figure S5. Evolution of the scattered light intensity with temperature of a solution of PGLu₂₃-*b*-ELP in pure water at 1 g.L⁻¹ (values obtained by DLS light scattering measurements at 90°).

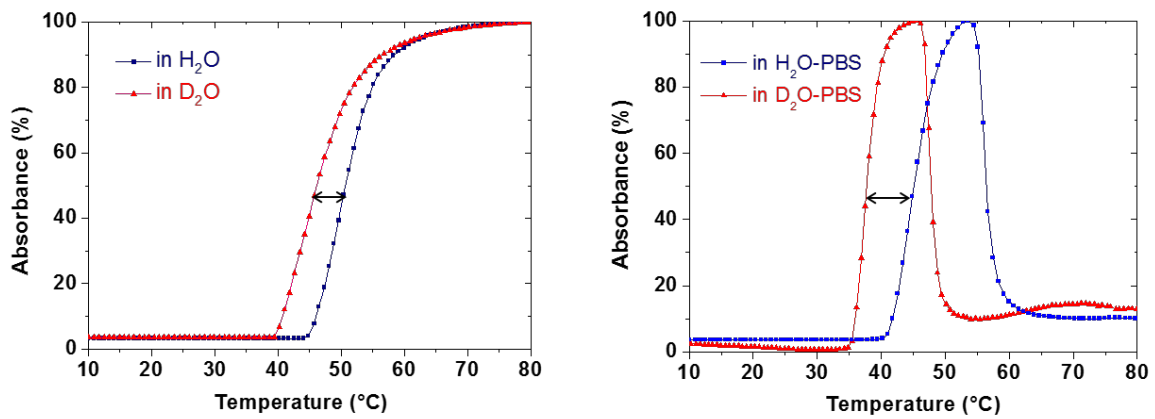


Figure S6. Evolution of absorbance of solutions of PGLu₂₃-*b*-ELP diblock copolyptide with temperature at 1 g.L⁻¹ in H₂O and in D₂O (left) and in H₂O-PBS and D₂O-PBS (right).

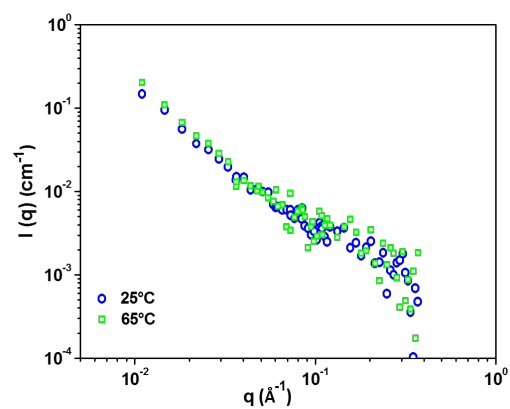


Figure S7. Small-angle neutron scattering intensity as a function of q for PGLu₂₃-*b*-ELP solution at 1 mg.mL⁻¹ in D₂O at 25°C (< T_t) and at 65°C (> T_t).

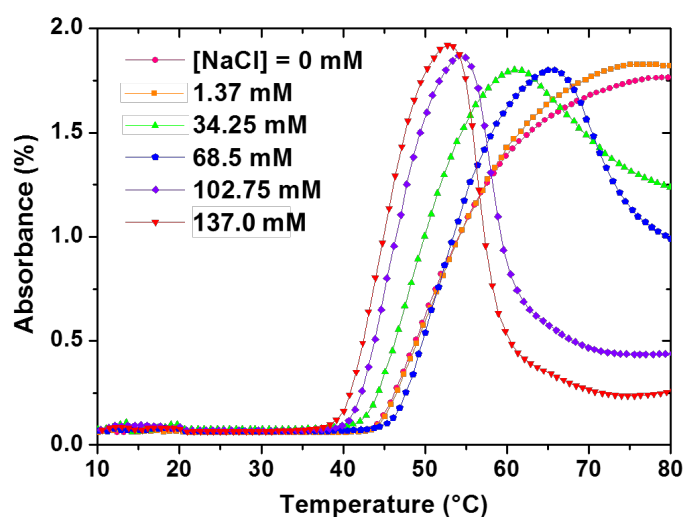


Figure S8. Evolution of absorbance of solutions of PGLu₂₃-*b*-ELP with temperature at 1.g.L⁻¹ in a phosphate buffer (Na₂HPO₄ 8 mM, KH₂PO₄ 2 mM, pH = 7.2) and different concentrations of NaCl (from 0 to 137 mM).

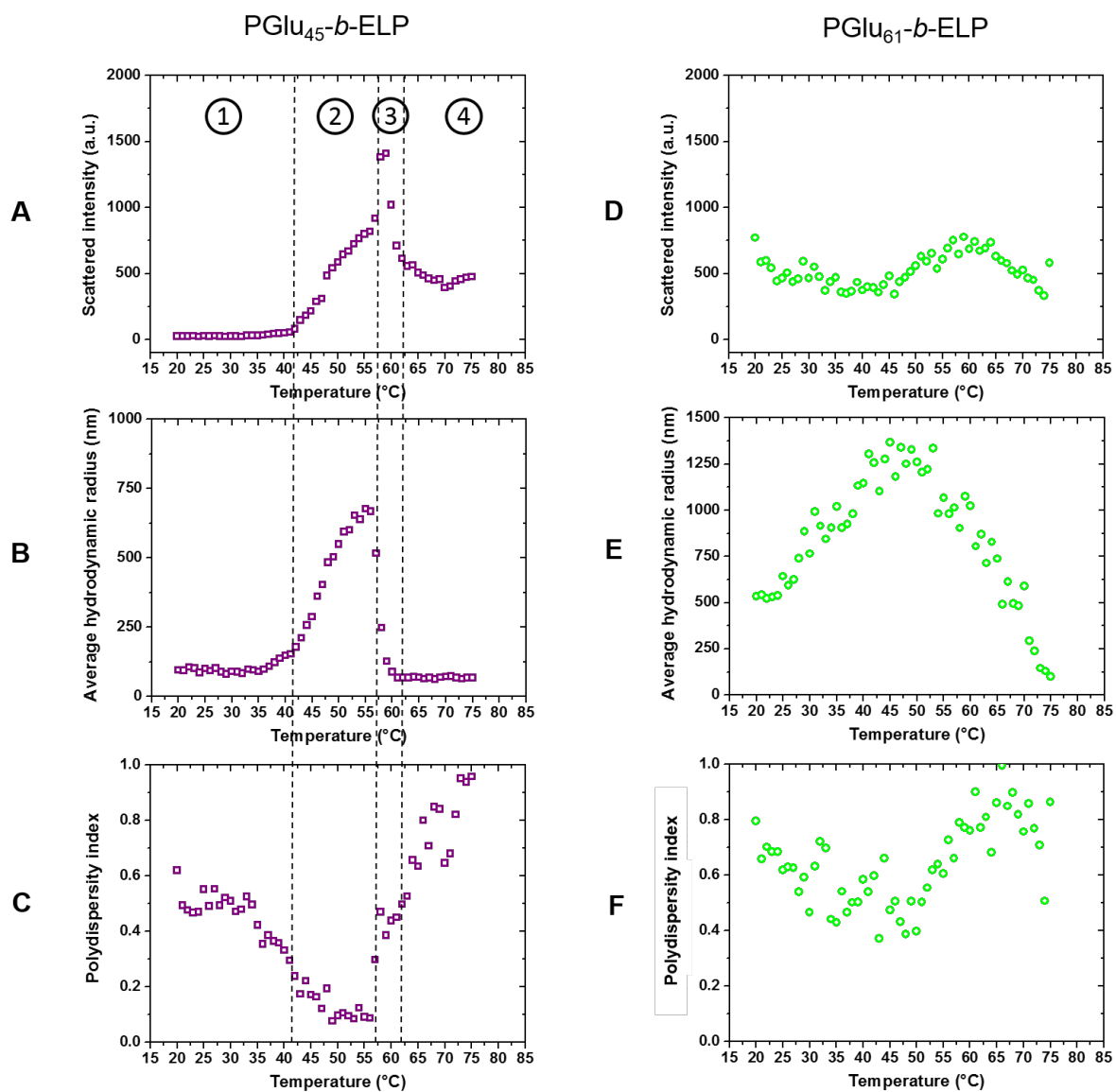


Figure S9. (A, D) Scattered light intensity, (B, E) average hydrodynamic radius and (C, F) polydispersity index *versus* temperature of solutions of PGlu₄₅-b-ELP (left) and PGlu₆₁-b-ELP (right) diblock copolypeptides at 1 g.L⁻¹ in PBS (values obtained by DLS measurements at 90°).

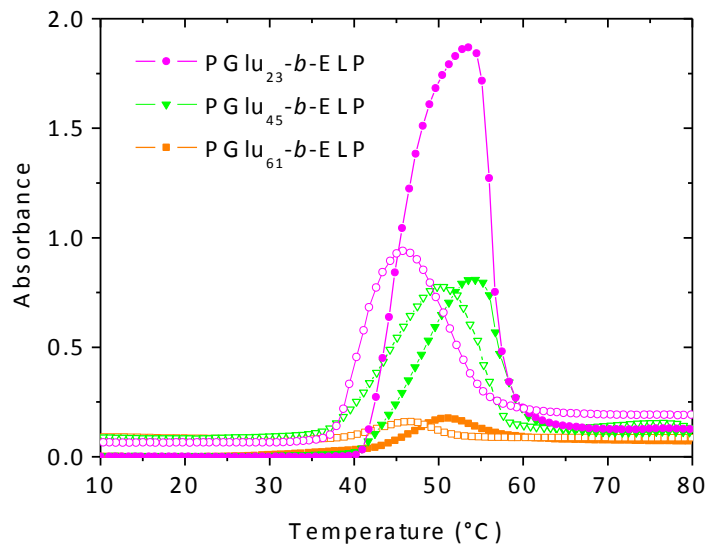


Figure S10. Evolution of absorbance with temperature of solutions of PGlu₂₃-*b*-ELP, PGlu₄₅-*b*-ELP and PGlu₆₁-*b*-ELP diblock copolypeptides at 1 g.L⁻¹ in PBS during heating (filled symbols) and cooling (empty symbols) to demonstrate reversible phase behavior.

The SANS curve for the copolypeptide P_{Glu₆₁}-*b*-ELP obtained at 45 °C (Figure S8, panel B) was not fitted using a polydisperse Sphere Model due to the presence of free chains with the nanoaggregates but using a mixed model of the polydisperse Sphere and the Debye models. Indeed, the Debye model is used to describe polymer chains in solution. For individual chains, the volume V_{part} is defined by M_w the weight-average molar mass of one mole of chains, M_0 the molar mass and v the volume of one repeating unit as $V_{\text{chain}} = M_w \cdot v / M_0$. Thus, for a dilute solution of polymer of weight concentration C , occupying a volume fraction $\Phi = N_A \cdot v \cdot C / M_0$, where N_A is the Avogadro number, and with $d = M_0 / (N_A \cdot v)$ Equation 1 becomes the Equation 2:

$$I(q) = \Phi \Delta \rho^2 V_{\text{part}} P(q) \quad \text{Equation 1}$$

$$I(q) = v^2 \Delta \rho^2 \frac{C}{M_0^2} N_A M_w P(q) = \Delta \rho^2 \frac{C}{d^2 N_A} M_w P(q) \quad \text{Equation 2}$$

The weight-average molar mass M_w and the radius of gyration R_g can be deduced from the fit to this equation using the Debye function¹ as form factor $P(q, R_g)$ (Equation 3):

$$P_{\text{Debye}}(q, R_g) = \frac{2}{(q^2 R_g^2)} (\exp(-q^2 R_g^2) + q^2 R_g^2 - 1) \quad \text{Equation 3}$$

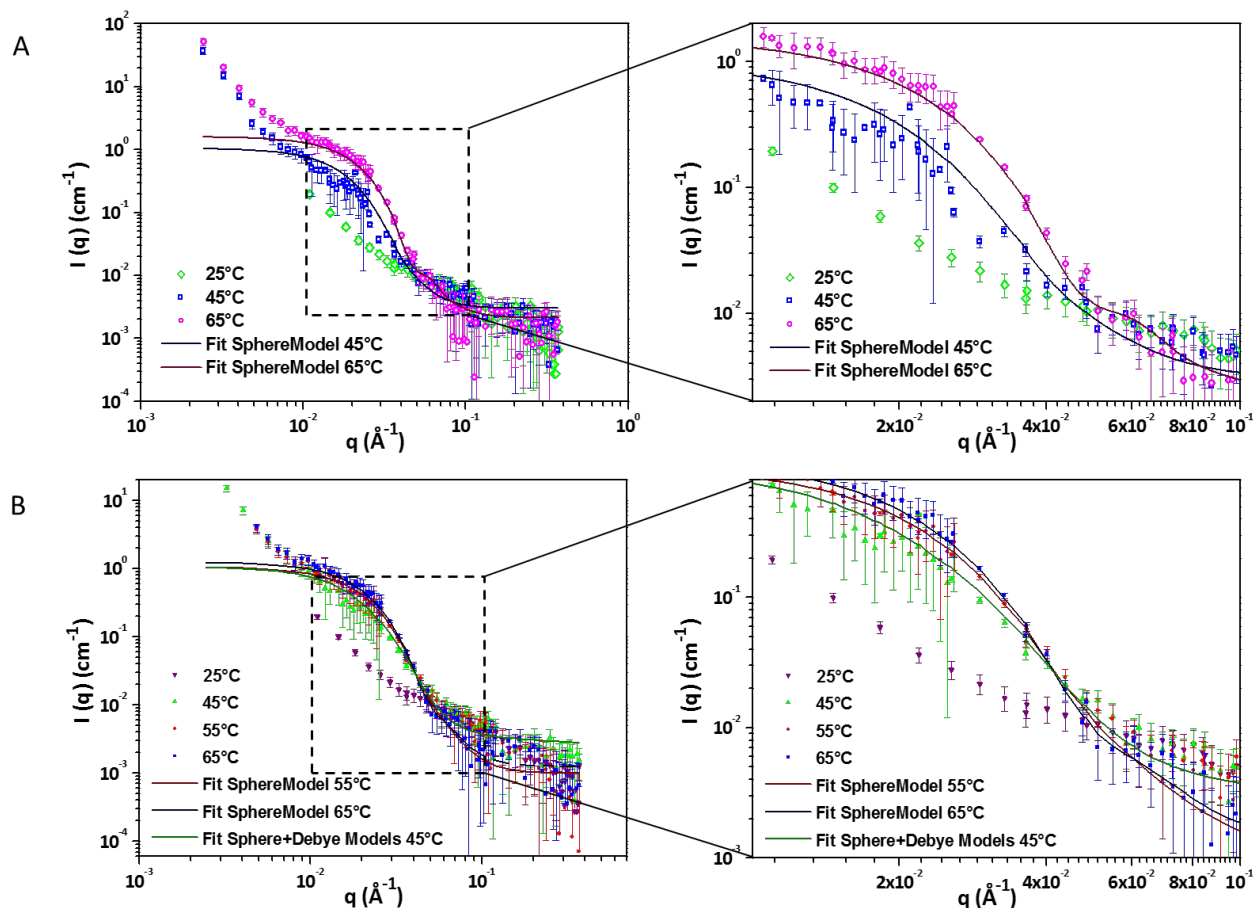


Figure S11. Small-angle neutron scattering of solutions of PGlu-*b*-ELP diblock copolypeptides prepared at $1 \text{ mg}\cdot\text{mL}^{-1}$ in D_2O -PBS. **(A)** Scattering intensity as a function of q for PGlu₄₅-*b*-ELP at various temperatures; the solid lines are the fitting curves by a polydisperse Sphere Model. **(B)** Scattering intensity as a function of q for PGlu₆₁-*b*-ELP at various temperatures; the solid lines are the fitting curves obtained by using a polydisperse sphere model (except for the data obtained at 45°C , the model used is a mixed model of the polydisperse Sphere and the Debye models).

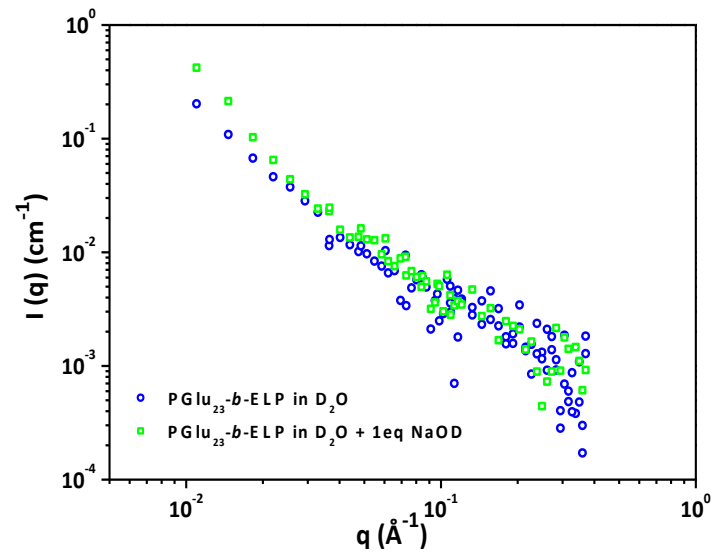


Figure S12. Small-angle neutron scattering intensity as a function of q for PGLu₂₃-b-ELP solution at $1 \text{ mg}\cdot\text{mL}^{-1}$ in D₂O and in D₂O with 1 eq of NaOD / carboxylic acid group (pD = 9) at $65 \text{ }^\circ\text{C}$ ($> T_t$).

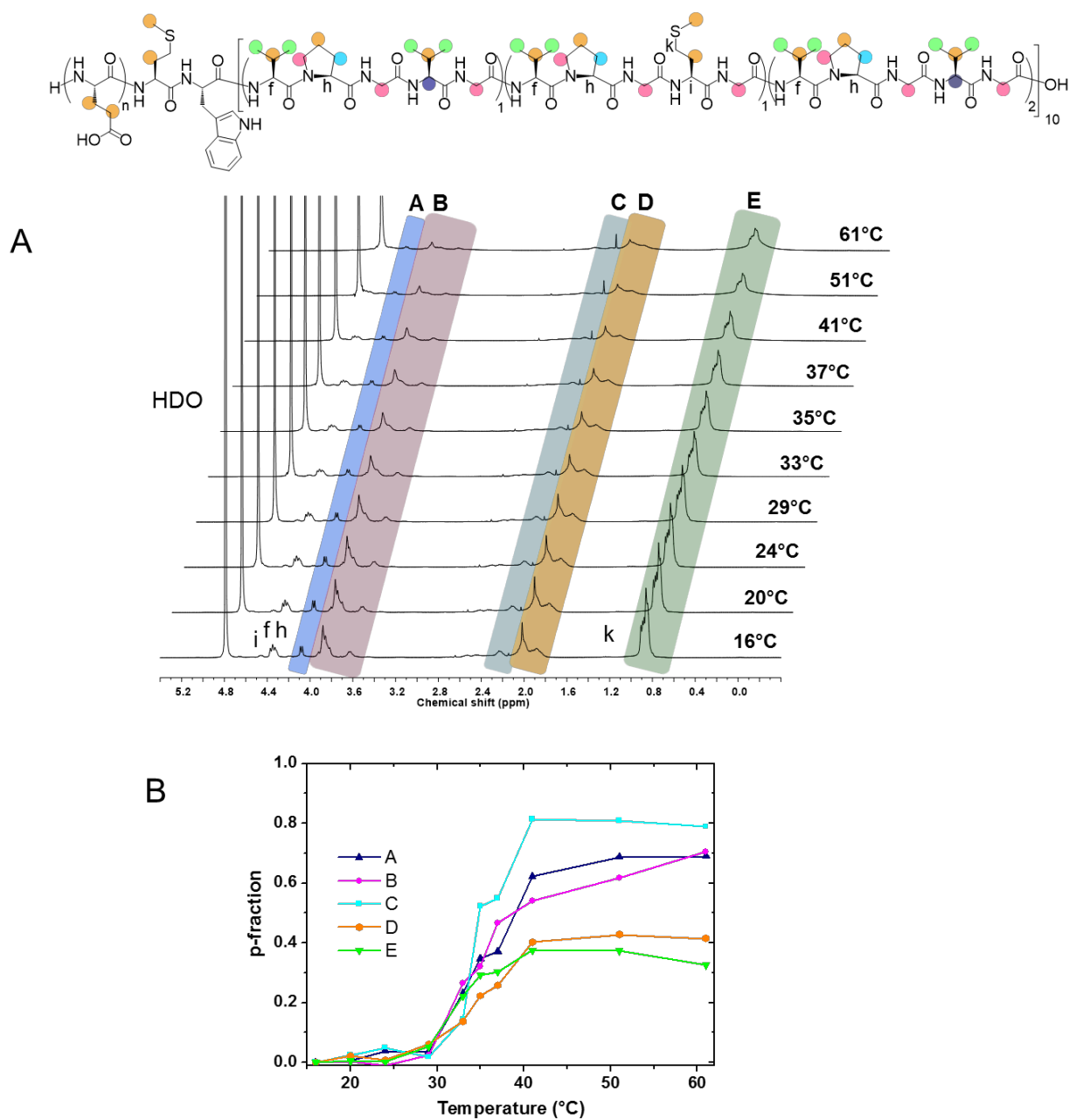


Figure S13. (A) ^1H NMR spectra of PGlu₂₃-*b*-ELP in D₂O (1 g.L⁻¹) at various temperatures. (B) Phase separation p-fraction from ^1H NMR signals A, B, C, D and E plotted as a function of the temperature.

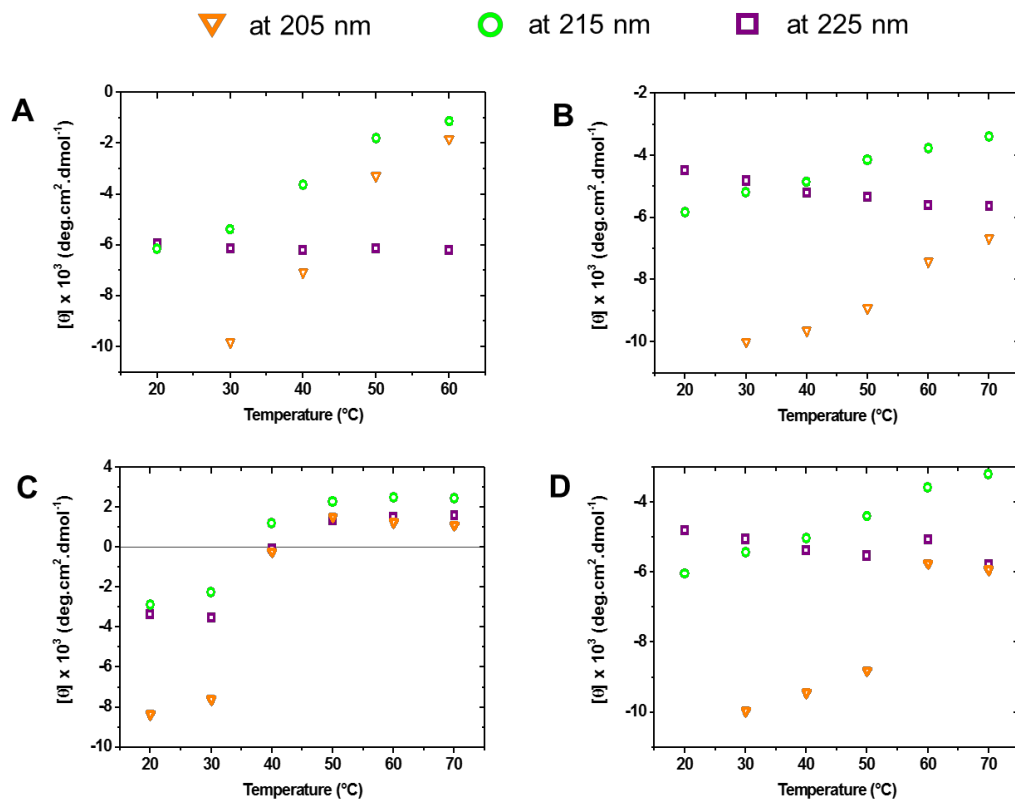


Figure S14. Temperature-dependence of the mean molar residue ellipticities at 205 nm, 215 nm and 225 nm of ELP in pure water (**A**) PGLu₂₃-*b*-ELP in pure water (**B**) and ELP in PBS (**C**) and PGLu₂₃-*b*-ELP in PBS (**D**) at 9 μM.

REFERENCES

- (1) Debye, P. Molecular-weight determination by light scattering. *The Journal of Physical Chemistry* **1947**, *51*, 18-32.